nature communications

Article

https://doi.org/10.1038/s41467-025-60302-6

Bioenergetic stress potentiates antimicrobial resistance and persistence

Received: 19 July 2024

Accepted: 15 May 2025

Published online: 09 June 2025

Check for updates

Barry Li[1,2], Shivani Srivastava[1,2], Mustafa Shaikh[1,2], Gautam Mereddy[1,2], Madison R. Garcia[1,3], Eric N. Chiles[4], Avi Shah[1,2], Boatema Ofori-Anyinam[1,2], Ting-Yu Chu[1,2], Nicole J. Cheney[1,2], Douglas McCloskey[5,7], Xiaoyang Su[4,6] & Jason H. Yang[1,2]

The bactericidal action of some antibiotics is associated with increased ATP consumption, cellular respiration, and reactive oxygen species (ROS) formation. Here, we investigate the effects of 'bioenergetic stress', induced by constitutive hydrolysis of ATP and NADH, on antibiotic efficacy in *Escherichia coli*. We show that bioenergetic stress potentiates the evolution of antibiotic resistance via enhanced ROS production, mutagenic break repair, and transcription-coupled repair. In addition, bioenergetic stress potentiates antibiotic persistence via the stringent response. We propose a model in which the balance between ATP consumption versus production regulates antibiotic resistance and persistence.

Antimicrobial resistance (AMR) is a global health crisis and poses a looming threat to modern medicine. Antimicrobial-resistant infections are estimated to have been associated with 4.95 million global deaths and have been directly responsible for 1.27 million global deaths in 2019[1]. Thus, there is an urgent need to better understand AMR mechanisms.

AMR is defined as heritable protection from antimicrobial agents. Resistance arises from de novo mutations or horizontally transferred mobile genetic elements that inhibit drug-target interactions or alter intracellular drug accumulation[2]. In the case of tuberculosis, resistance can only be acquired by de novo mutations[3]. In addition, non-heritable forms of protection from antimicrobial agents exist, including antimicrobial persistence[4]. Persistence arises from isogenic subpopulations of "persister cells" that exhibit prolonged survival under bactericidal stress[5–8]. Persistence can facilitate downstream resistance evolution[9–12].

Mechanisms underlying antibiotic-induced resistance and persistence are poorly understood[13,14]. Mostly studied in *Escherichia coli*, growing evidence demonstrates that antibiotic treatment exerts pleiotropic stresses that can potentiate mutation rates, thereby enabling AMR evolution (stress-induced mutagenesis)[10,11,15–20]. Such stresses alter bacterial physiology and can amplify metabolic processes, including ATP consumption[21–24], cellular respiration[25,26], and the production of reactive oxygen species (ROS)[24,25,27]. When ATP consumption exceeds ATP production, cells experience "bioenergetic stress".

Here, we define bioenergetic stress as the state where the ATP/ADP ratio and the adenylate energy charge (AEC, a quantitative measure of the energy status of a cell)[28] are decreased. Several conditions induce bioenergetic stress, including heterologous gene expression[29] hypoxic stress[30], oxidative stress[31], or acid stress[32]. Bioenergetic stress impairs growth and enhances glycolysis, oxidative phosphorylation, and ROS formation in *E. coli*[33–38]. Excessive ROS accumulation stimulates stress-induced mutagenesis via multiple DNA repair mechanisms[39]; molecules that inhibit ROS decelerate AMR evolution[17,18]. Antimicrobial persistence is associated with decreased central carbon metabolism and depleted intracellular ATP[5,8,40–45]. However, while antibiotic-induced ROS formation is well-studied[13,14,27,46], it is unknown if and how bioenergetic stress regulates resistance and persistence[47].

Here, we utilized a synthetic biology approach to directly study how bioenergetic stress impacts antimicrobial resistance and

[1]Center for Emerging and Re-emerging Pathogens, Rutgers New Jersey Medical School, Newark, NJ, USA. [2]Department of Microbiology, Biochemistry, and Molecular Genetics, Rutgers New Jersey Medical School, Newark, NJ, USA. [3]Department of Biochemistry; Rutgers University, The State University of New Jersey, New Brunswick, NJ, USA. [4]Rutgers Cancer Institute of New Jersey; Rutgers University, The State University of New Jersey, New Brunswick, NJ, USA. [5]Novo Nordisk Foundation Center for Biosustainability, Technical University of Denmark, Lyngby, Denmark. [6]Department of Medicine, Rutgers Robert Wood Johnson Medical School, New Brunswick, NJ, USA. [7]Present address: BioMed X Institute, Heidelberg, Germany. e-mail: jason.y@rutgers.edu

persistence in *E. coli*. We found that bioenergetic stress accelerates fluoroquinolone resistance evolution via a stress-induced mutagenesis mechanism involving ROS, mutagenic break repair, and transcription-coupled repair. We also found that bioenergetic stress potentiates persister cell formation via the stringent response and that the stringent response contributes to bioenergetic stress-enhanced resistance evolution. We propose a model for how antibiotic stress can enhance antimicrobial resistance and persistence by altering bacterial energetics.

Results

Bioenergetic stress enhances antibiotic resistance evolution and persistence

Our previous work implicates antibiotic-induced ATP consumption as an inducer of hyper-respiratory activity[21]. To determine if antibiotic treatment induces bioenergetic stress, we metabolically profiled antibiotic-treated *E. coli* MG1655 cells by LC-MS/MS[48,49] (Supplementary Data 1). One hour treatment with 16 ng/mL of the fluoroquinolone ciprofloxacin (~2x the minimum inhibitory concentration [MIC]) significantly decreased intracellular ATP and NADH, resulting in decreased ATP/ADP, AEC, and NADH/NAD^+ (Fig. 1a). The greatest metabolomic changes occurred in nucleotides (thymine, dNTPs, dNDPs, dNMPs) and pentose phosphate pathway metabolites (ribulose-5-phosphate, sedoheptulose 7-phosphate). Accumulation of these metabolites significantly increased, consistent with ciprofloxacin's mechanism of action and supporting our previous findings that nucleotide metabolism significantly contributes to antibiotic lethality[21].

To investigate the direct effects of bioenergetic stress on antibiotic efficacy without the confounding effects of pleiotropic changes in bacterial physiology induced by antibiotic treatment, we took a synthetic biology approach. We engineered a genetic system comprised of constitutive over-expression of *E. coli*'s soluble ATP synthase F_1 complex (*atpAGD*; pF_1), constitutive heterologous expression of the *Streptococcus pneumoniae* NADH oxidase (*nox*; pNOX), and empty vector controls (pEmpty) on low-copy plasmids[34–38]. Expression of *atpAGD* or *nox* induces continuous ATP hydrolysis or NADH oxidation, respectively. This increases ATP or NADH consumption, decreasing ATP/ADP or NADH/NAD^+, and thus creates bioenergetic stress. These bioenergetic ratios are key indicators of a cell's energy state[50] and redox state[51], respectively, and are key regulators of biochemistry and bacterial physiology[52–54].

To validate this system, we quantified the abundance of intracellular ATP, ADP, and AMP by LC-MS/MS (Supplementary Data 2) and NAD^+ and NADH using the Promega NAD/NADH-Glo assay. Consistent with expectations, ATP/ADP and AEC were significantly decreased in pF_1 cells, and NADH/NAD^+ was significantly decreased in pNOX cells, relative to pEmpty controls (Fig. 1b). ATP/ADP and AEC were also decreased in pNOX cells. Consistent with previous reports[33–38], pF_1 and pNOX cells exhibited extended lag phase (Fig. 1c), enhanced respiration (Fig. 1d and Supplementary Fig. 1a; increased OCR: oxygen consumption rate), and enhanced glycolysis (Fig. 1e and Supplementary Fig. 1b; increased ECAR: extracellular acidification rate) than pEmpty cells. Moreover, LC-MS/MS analyses revealed significantly increased accumulation of tricarboxylic acid cycle metabolites (α-ketoglutarate, citrate, fumarate, malate, succinate) or their related metabolites (coenzyme A, pyruvate) in pF_1 and/or pNOX cells (Supplementary Data 2). Together, these data validated our genetic system.

We evaluated the effects of bioenergetic stress on antibiotic susceptibility and treatment outcomes. The ciprofloxacin MIC was not altered in pF_1 or pNOX cells relative to pEmpty cells, indicating that this level of bioenergetic stress did not directly confer genetic resistance (Fig. 1f). However, serial passage laboratory evolution experiments revealed statistically significantly enhanced ciprofloxacin resistance evolution in pF_1 cells and modestly enhanced resistance evolution in pNOX cells relative to pEmpty cells (Fig. 1g). These were evident in both the area under the curve (AUC) of the fold-change in MIC_{50} throughout the experiment and the cycles to 4x MIC_{50} (Supplementary Fig. 1c). We selected 4x MIC_{50} as the resistance threshold, as a 4-fold increased MIC is the resistance breakpoint for many antibiotics[55]. These data indicate that bioenergetic stress accelerates ciprofloxacin resistance evolution. This finding was unexpected as, to our knowledge, bioenergetic stress has never been directly shown to impose a selective pressure that enhances antimicrobial resistance evolution.

We performed time-kill experiments to evaluate the potential effects of bioenergetic stress on antibiotic lethality. Time-kill experiments revealed statistically significant increases in the fraction of cells surviving 18 ng/mL ciprofloxacin treatment (~1.5 x MIC) in bioenergetically stressed cells, indicating enhanced persistence[7] (Fig. 1h and Supplementary Fig. 1d). We selected 18 ng/mL ciprofloxacin because this concentration yielded ~ 3-logs killing in pEmpty cells, like 16 ng/mL ciprofloxacin in wildtype MG1655 cells (Supplementary Fig. 1e). These concentrations enabled us to resolve both log-fold increases and decreases in antibiotic lethality following genetic and/or biochemical perturbations. We found that the increased persistence was a generalizable phenomenon, with significantly elevated pF_1 persister cell fractions surviving high doses of ciprofloxacin, gentamicin, and ampicillin, and significantly elevated pNOX persister cell fractions surviving high doses of ciprofloxacin and gentamicin (Supplementary Fig. 1f–h). These results were surprising as we had previously found that elevated respiration was associated with enhanced antibiotic lethality and decreased persistence[21,26]. Together, these data reveal that bioenergetic stress enhances both genotypic and phenotypic AMR.

Bioenergetic stress induces oxidative DNA damage

To understand how bioenergetic stress alters bacterial physiology, we sequenced RNA from exponential-phase bioenergetically stressed pF_1 and pNOX cells and pEmpty control cells. Importantly, sequencing analyses revealed increased expression of *atpA*, *atpG*, and *atpD* in only pF_1 and expression of *nox* in only pNOX cells (Supplementary Fig. 2a–c). Statistical analyses revealed 72 differentially expressed genes (DEGs; ≥ 2-fold change, FDR-corrected $p \leq 0.05$) between pF_1 and pEmpty cells and 314 DEGs between pNOX and pEmpty cells (Supplementary Data 3). Consistent with our observation that ATP/ADP and AEC were decreased in both pF_1 and pNOX cells, all DEGs in pF_1 cells were also differentially expressed in pNOX cells. However, we did not find any significant changes in the expression of DNA repair, oxidative stress response, or stringent response genes (Supplementary Data 4). This was unexpected because these pathways are implicated as mechanisms of antimicrobial resistance evolution[39] and persistence[6].

Gene Ontology analyses of the 72 DEGs revealed significant upregulation of genes involved in chemotaxis and flagellar assembly and downregulation of genes involved in hydrogen sulfide metabolism (Supplementary Data 5 and Supplementary Fig. 2d). The decreased expression of H_2S metabolism genes (*cys* regulon) was surprising because H_2S protects against bactericidal antibiotics[56,57]. Because chemotaxis and motility are major sources of ATP consumption[58,59], we hypothesized that deletion of CheY or FlhD, the transcription factors regulating the expression of chemotaxis or flagellar assembly genes, could reverse bioenergetic stress-enhanced persistence and thus increase ciprofloxacin lethality in pF_1 and pNOX cells. However, bioenergetic stress-enhanced persistence was not rescued in Δ*cheY* or Δ*flhD* cells (Supplementary Fig. 2e).

Because bioenergetic stress alters bacterial metabolism[33–38], we performed genome-scale metabolic modeling analyses[60] to predict how bioenergetic stress would globally remodel *E. coli* metabolism (Supplementary Data 6). We applied our RNA sequencing data as modeling constraints[61,62] to the comprehensive iML1515 genome-scale

https://doi.org/10.1038/s41467-025-60302-6

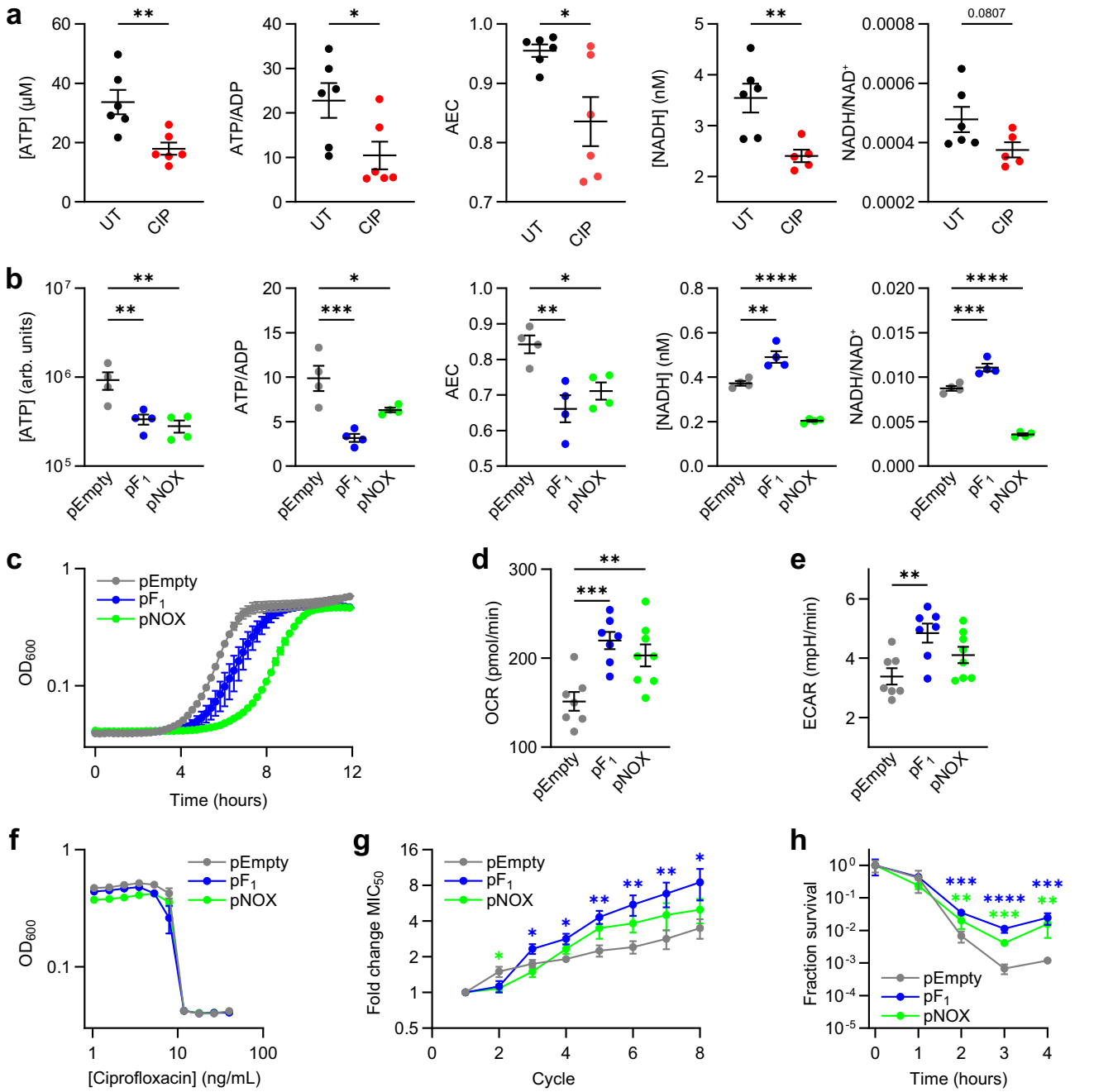

model of *E. coli* metabolism[63] and performed flux balance analysis. Consistent with the expectation that bioenergetically stressed cells induce compensatory ATP and NADH production, model simulations predicted increased ATP synthase activity and NADH production in both pF_1 and pNOX cells over pEmpty cells (Fig. 2a). Notably, model simulations also predicted increased both oxygen consumption and hexokinase activity (the first step of glycolysis), indicating enhanced activity in both oxidative and substrate-level phosphorylation (Fig. 2b). Consistent with these model predictions, both pF_1 and pNOX cells possessed increased accumulation of tricarboxylic acid cycle metabolites (Supplementary Data 2) and enhanced OCR and ECAR (Figs. 1d, e) than pEmpty cells. Interestingly, while the model predicted higher hexokinase activity in pNOX cells than in pF_1 cells (Fig. 2b), we found that ECAR increased less in pNOX cells than in pF_1 cells (Fig. 1e), suggesting that pNOX cells rely less on fermentation than pF_1 cells (possibly because NADH oxidase directly regenerates NAD^+). Collectively, these experimental results validated our model.

Although the expression of the oxidative stress response regulators *oxyR*, *oxyS*, *soxR*, or *soxS* did not significantly increase (Supplementary Data 3 and 4, Supplementary Fig. 3), model simulations predicted significantly increased H_2O_2 production, catalase activity, superoxide production, and superoxide dismutase activity (Fig. 2c). These results suggested that bioenergetic stress increases ROS production. To test this model prediction, we used a highly specific and quantitative assay that measures changes in H_2O_2 production[64]. This assay uses horseradish peroxidase and Amplex UltraRed to quantify extracellular H_2O_2 accumulation generated by catalase and peroxidase-deficient Δ*ahpCF* Δ*katG* Δ*katE* (ΔHPX). These cells are unable to detoxify H_2O_2, and H_2O_2 rapidly equilibrates across the plasma membrane. Thus, nearly all H_2O_2 generated by these cells can be assayed by sampling the extracellular media. We introduced pF_1, pNOX, and pEmpty plasmids into ΔHPX cells and observed enhanced H_2O_2 production in both ΔHPX pF_1 and ΔHPX pNOX cells relative to ΔHPX pEmpty

Fig. 1 | Bioenergetic stress potentiates antimicrobial resistance evolution and persistence. a Energetic metabolite profiles for untreated (UT) and ciprofloxacin treated (CIP) *E. coli* MG1655 cells as determined by LC-MS/MS. Exponential phase cells were grown in MOPS minimal media and treated with ± 16 ng/mL ciprofloxacin for 1 h ($n = 6$). ($p = 0.0066$ for [ATP], 0.0335 for ATP/ADP, 0.0186 for adenylate energy charge [AEC], 0.0074 for [NADH], and 0.0807 for NADH/NAD^+ by two-sided unpaired t-tests). **b** Energetic metabolite profiles for pEmpty, pF_1, and pNOX cells grown in MOPS-rich media as determined by LC-MS/MS or Promega NAD/NADH-Glo ($n = 4$). Statistical testing by one-way ANOVA with Dunnett's multiple comparisons test versus pEmpty for [ATP] ($p = 0.0035$; pF_1 $p = 0.0088$, pNOX $p = 0.0030$), ATP/ADP ($p = 0.0014$; pF_1 $p = 0.0008$, pNOX $p = 0.0318$), AEC ($p = 0.0055$; pF_1 $p = 0.0037$, pNOX $p = 0.0227$), [NADH] ($p < 0.0001$; pF_1 $p = 0.0012$, pNOX $p < 0.0001$), and NADH/NAD^+ ($p < 0.0001$; pF_1 $p = 0.0007$, pNOX $p < 0.0001$). **c** Growth curves for pEmpty, pF_1, and pNOX cells grown in MOPS-rich media ($n = 4$). **d** Exponential phase oxygen consumption rates (OCR) as a reporter of respiratory activity ($n = 7$ for pEmpty and pF_1; $n = 8$ for pNOX). Statistical testing by one-way ANOVA ($p = 0.0011$) with Dunnett's multiple comparisons test versus pEmpty (pF_1 $p = 0.0008$, pNOX $p = 0.0068$). **e** Exponential phase extracellular acidification rates (ECAR) as a reporter of glycolytic activity ($n = 7$ for pEmpty and pF_1; $n = 8$ for pNOX). Statistical testing by one-way ANOVA ($p = 0.0097$) with Dunnett's multiple comparisons test versus pEmpty (pF_1 $p = 0.0050$, pNOX $p = 0.1621$). **f** Growth of $OD_{600} = 0.0001$ exponential phase cells in the presence of ciprofloxacin ($n = 4$). **g** Ciprofloxacin resistance evolution for pEmpty, pF_1, and pNOX cells over 8 cycles of serial-passage ($n = 12$). Data reported as change in the minimum concentration for 50% growth inhibition (MIC_{50}) relative to Cycle 1. Statistical testing by two-way ANOVA ($p = 0.0150$) with Dunnett's multiple comparisons test versus pEmpty (Cycle 1: not determined; Cycle 2: pF_1 $p = 0.1097$, pNOX $p = 0.0490$; Cycle 3: pF_1 $p = 0.0448$, pNOX $p = 0.3654$; Cycle 4: pF_1 $p = 0.0170$, pNOX $p = 0.1550$; Cycle 5: pF_1 $p = 0.0012$, pNOX $p = 0.1447$; Cycle 6: pF_1 $p = 0.0014$, pNOX $p = 0.0817$; Cycle 7: pF_1 $p = 0.0099$, pNOX $p = 0.2457$; Cycle 8: pF_1 $p = 0.0429$, pNOX $p = 0.4146$). **h** Ciprofloxacin lethality following treatment with 18 ng/mL ciprofloxacin ($n = 4$). Data reported as change in colony-forming units (CFUs) relative to time 0. Data depicted as mean ± 95% CI. Statistical testing by two-way ANOVA ($p < 0.0001$) with Dunnett's multiple comparisons test versus pEmpty (0 h: pF_1 $p = 0.9986$, pNOX $p = 0.9722$; 1 h: pF_1 $p = 0.7873$, pNOX $p = 0.1278$; 2 h: pF_1 $p = 0.0007$, pNOX $p = 0.0021$; 3 h: pF_1 $p < 0.0001$, pNOX $p = 0.0004$; 4 h: pF_1 $p = 0.0002$, pNOX $p = 0.0014$). All experiments performed in MOPS-rich media unless otherwise indicated. All data represent biological replicates (independent cultures) and are depicted as mean ± SEM unless otherwise indicated. $^*p \le 0.05$, $^{**}p \le 0.01$, $^{***}p \le 0.001$, $^{****}p \le 0.0001$. $p \ge 0.1$ not shown. Source data are provided within the 'Source Data.xlsx' file.

controls (Fig. 2d). These results were consistent with previous findings that ATP futile cycling enhances H_2O_2 production[37].

We examined the expression of oxidative stress response genes in the RNA sequencing data and found significant changes in only the expression of the *katE* catalase gene, which is regulated by RpoS[65] and which was increased in only pNOX cells (Supplementary Data 4). The lack of induction of OxyR or SoxRS was surprising. This suggested that pF_1 and pNOX cells did not mount a strong protective oxidative stress response despite experiencing increased ROS production. Thus, we hypothesized that bioenergetically stressed cells would accumulate oxidative damage to cellular components. To test this hypothesis, we performed enzyme-linked immunosorbent assays (ELISAs) for carbonylated proteins and 8-oxo-deoxyguanosine (8-oxo-dG) and found enhanced oxidative damage to proteins (Fig. 2e) and DNA (Fig. 2f) in pF_1 and pNOX cells over pEmpty cells. These results are interesting because they show that even in the absence of exogenous stress, bacteria can experience levels of oxidative stress that are sufficient for cellular damage but not for activating canonical oxidative stress responses[66]. Importantly, these results revealed that bioenergetic stress induces oxidative DNA damage, which is highly mutagenic[67].

Bioenergetic stress accelerates resistance evolution via enhanced ROS production

We hypothesized that the enhanced 8-oxo-dG accumulation in pF_1 and pNOX cells was accelerating ciprofloxacin resistance evolution by increasing their basal mutation rates. To test this hypothesis, we performed Luria-Delbrück fluctuation tests[68,69]. Surprisingly, basal mutation rates did not differ between pF_1, pNOX, and pEmpty cells (Fig. 3a). This suggested that bioenergetic stress-accelerated resistance evolution was caused by stress-induced mutagenesis. To test this secondary hypothesis, we performed fluctuation tests in media containing 8 ng/mL ciprofloxacin (~0.67 x MIC). We found that stress-induced mutation rates and the relative increase in stress-induced versus non-stress-induced mutation rates were significantly higher in pF_1 and pNOX cells than in pEmpty cells (Fig. 3b). Together, these data indicate that bioenergetic stress enhances stress-induced mutagenesis.

Oxidative stress enhances stress-induced mutagenesis[10,15]. Thus, we hypothesized that the physiological changes induced by bioenergetic stress (i.e., enhanced respiration and ROS production) mechanistically accelerated ciprofloxacin resistance evolution. We tested this hypothesis using both genetic and biochemical approaches. To genetically manipulate cellular respiration, we used Δ*atpA* or Δ*cyoA* Δ*cydB* Δ*appB* (ΔETC) cells, which increase or decrease respiratory activity, respectively (Fig. 3c and Supplementary Fig. 4a)[26,70,71]. Δ*atpA* cells lack ATP synthase F_1 complexes and synthesize ATP via substrate-level phosphorylation. In these cells, respiration is uncoupled and is increased to maintain redox balance by dissipating reducing equivalents formed from enhanced carbon catabolism[70]. Protons may flow through intact membrane-bound F_0 complexes to dissipate the proton gradient[72]. ΔETC cells lack functional cytochrome oxidase complexes and thus cannot respire. We expected enhanced respiration in Δ*atpA* cells to cause enhanced ROS accumulation. To test this hypothesis, we performed horseradish peroxidase-Amplex UltraRed, protein carbonylation ELISA, and 8-oxo-dG ELISA experiments and found enhanced H_2O_2 production, carbonylated proteins, and 8-oxo-dG accumulation in Δ*atpA* cells relative to their wild-type controls (Fig. 3d–f and Supplementary Fig. 4b). These data validated Δ*atpA* as an appropriate genetic model for enhanced respiration and ROS. To genetically manipulate ROS, we used ΔHPX cells. Using the same assays as above, we validated that ΔHPX cells possessed greater ROS production and oxidative cellular damage than wildtype controls (Fig. 3e, f and Supplementary Fig. 4b).

We performed laboratory evolution experiments with wildtype, Δ*atpA*, and ΔETC cells to determine if elevated respiration was sufficient for accelerating ciprofloxacin resistance evolution. We found that resistance evolution was modestly, but not statistically significantly, accelerated in high-respiring Δ*atpA* cells but not in low-respiring ΔETC cells (Fig. 3g and Supplementary Fig. 4c). We next performed laboratory evolution experiments with pF_1, pNOX, and pEmpty cells in the presence of 12.5 μM piceatannol to determine if elevated respiration was necessary for bioenergetic stress-enhanced resistance evolution. Piceatannol is an ATP synthase inhibitor[73] that decreases cellular respiration in *E. coli* without inhibiting growth (Supplementary Fig. 4d–f). ATP synthase inhibition by piceatannol blocks proton translocation, preventing dissipation of the proton gradient and impairing electron transport and respiration. We found that respiratory inhibition by piceatannol treatment inhibited accelerated ciprofloxacin resistance acquisition in pF_1 and pNOX cells (Fig. 3h and Supplementary Fig. 4g). These results suggest that increased respiration is a key component of bioenergetic stress-enhanced resistance evolution.

We next performed laboratory evolution experiments with wildtype and ΔHPX cells to determine if elevated ROS was sufficient for accelerating ciprofloxacin resistance evolution. Consistent with our hypothesis, ciprofloxacin resistance evolution was modestly, but not

https://doi.org/10.1038/s41467-025-60302-6

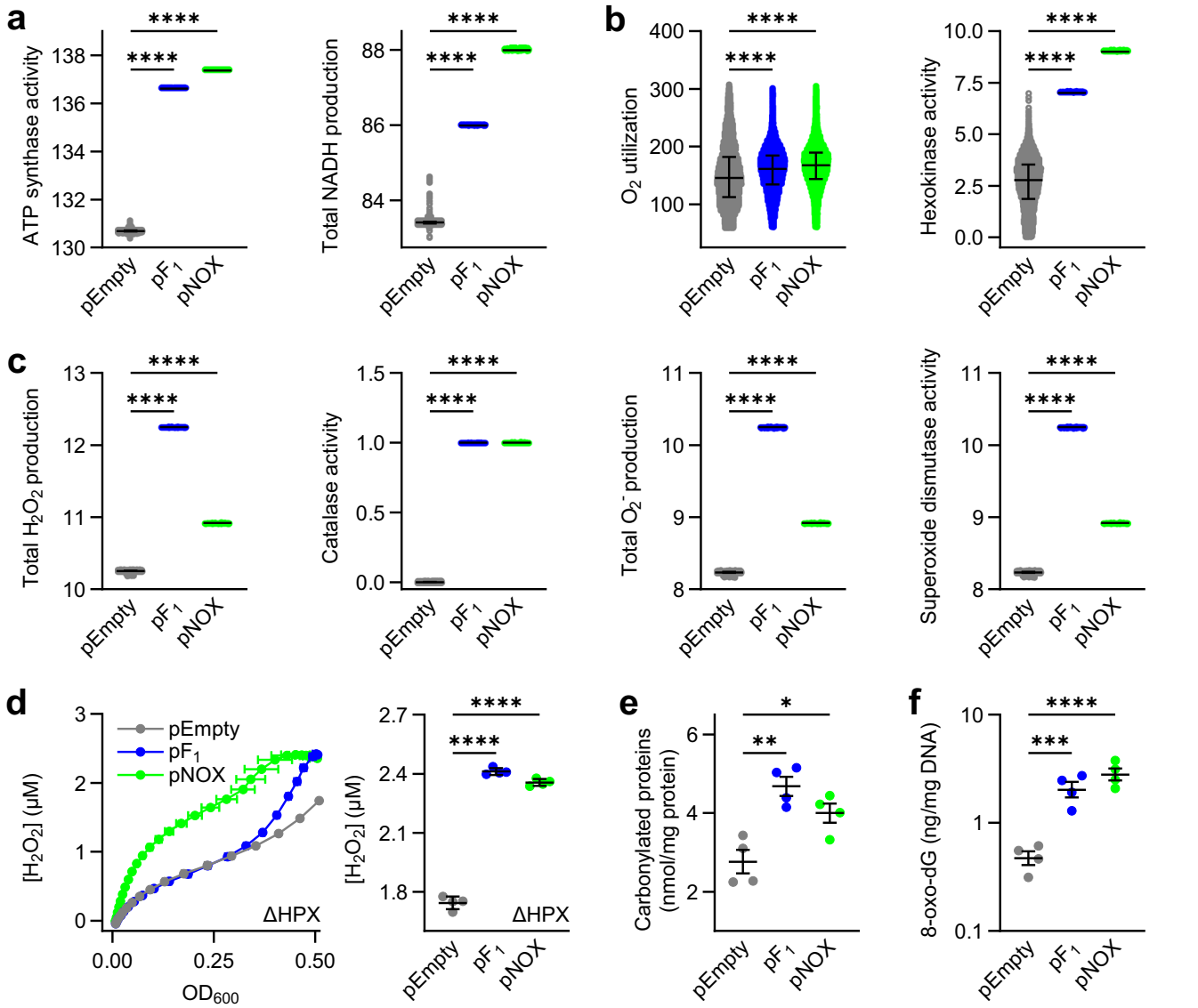

Fig. 2 | Bioenergetic stress induces oxidative cellular damage. a ATP synthase activity (*left*, $p < 0.0001$; pF_1 $p < 0.0001$, pNOX $p < 0.0001$) and NADH production rates (*right*, $p < 0.0001$; pF_1 $p < 0.0001$, pNOX $p < 0.0001$) predicted by genome-scale metabolic modeling using the iML1515 model of *E. coli* metabolism[63] ($n \geq 10{,}000$ flux samples for all model simulations). **b** Predicted respiratory (O_2 utilization, *left*, $p < 0.0001$; pF_1 $p < 0.0001$, pNOX $p < 0.0001$) and glycolytic (hexokinase, *right*, $p < 0.0001$; pF_1 $p < 0.0001$, pNOX $p < 0.0001$) activities. **c** Predicted intracellular H_2O_2 production ($p < 0.0001$; pF_1 $p < 0.0001$, pNOX $p < 0.0001$), catalase activity ($p < 0.0001$; pF_1 $p < 0.0001$, pNOX $p < 0.0001$), superoxide production ($p < 0.0001$; pF_1 $p < 0.0001$, pNOX $p < 0.0001$), and superoxide dismutase activity rates ($p < 0.0001$; pF_1 $p < 0.0001$, pNOX $p < 0.0001$). Statistical testing for modeling data by the Kruskal-Wallis test with Dunn's multiple comparisons test versus pEmpty. Error bars depict median flux distributions ± interquartile ranges. **d** Integrated H_2O_2 production by catalase and peroxidase-deficient Δ*ahpCF* Δ*katE* Δ*katG* (ΔHPX) cells expressing pEmpty, pF_1, or pNOX measured using a highly specific horseradish peroxidase and Amplex Red assay[64] (*left*). Integrated H_2O_2 at mid-exponential phase ($OD_{600} \approx 0.5$; *right*). Statistical testing by one-way ANOVA ($p < 0.0001$) with Šídák's multiple comparisons test versus pEmpty (pF_1 $p < 0.0001$, pNOX $p < 0.0001$). **e** Carbonylated proteins in exponential phase pEmpty, pF_1, ($p = 0.0011$) and pNOX ($p = 0.0164$) cells as determined by ELISA. Statistical testing by one-way ANOVA ($p = 00019$) with Dunnett's multiple comparisons test versus pEmpty. **f** Oxidized deoxyguanosine (8-oxo-dG) in exponential phase pEmpty, pF_1, ($p = 0.0001$) and pNOX ($p < 0.0001$) cells as determined by ELISA. Statistical testing by one-way ANOVA ($p < 0.0001$) with Dunnett's multiple comparisons test versus pEmpty. All experiments performed in MOPS-rich media. $n = 4$ for all experiments. All experimental data represent biological replicates (independent cultures) and are depicted as mean ± SEM. *$p \leq 0.05$, **$p \leq 0.01$, ***$p \leq 0.001$, ****$p \leq 0.0001$. Non-significant comparisons not shown. Source data are provided within the 'Source Data.xlsx' file.

statistically significantly, accelerated in ΔHPX cells relative to wild-type controls (Fig. 3i and Supplementary Fig. 4c). To determine if elevated ROS was necessary for bioenergetic stress-enhanced resistance evolution, we performed similar experiments in pF_1, pNOX, and pEmpty cells in the presence or absence of 15 U/mL catalase. We found that ROS detoxification by catalase prevented accelerated ciprofloxacin resistance acquisition in pF_1 and pNOX cells (Fig. 3j and Supplementary Fig. 4h).

Together, these results reveal that the increased respiration and ROS accumulation induced by bioenergetic stress causally accelerates antimicrobial resistance evolution.

Bioenergetic stress-enhanced persistence requires the stringent response

We next sought to understand how bioenergetic stress potentiates antimicrobial persistence. To determine if persistence, like accelerated

https://doi.org/10.1038/s41467-025-60302-6

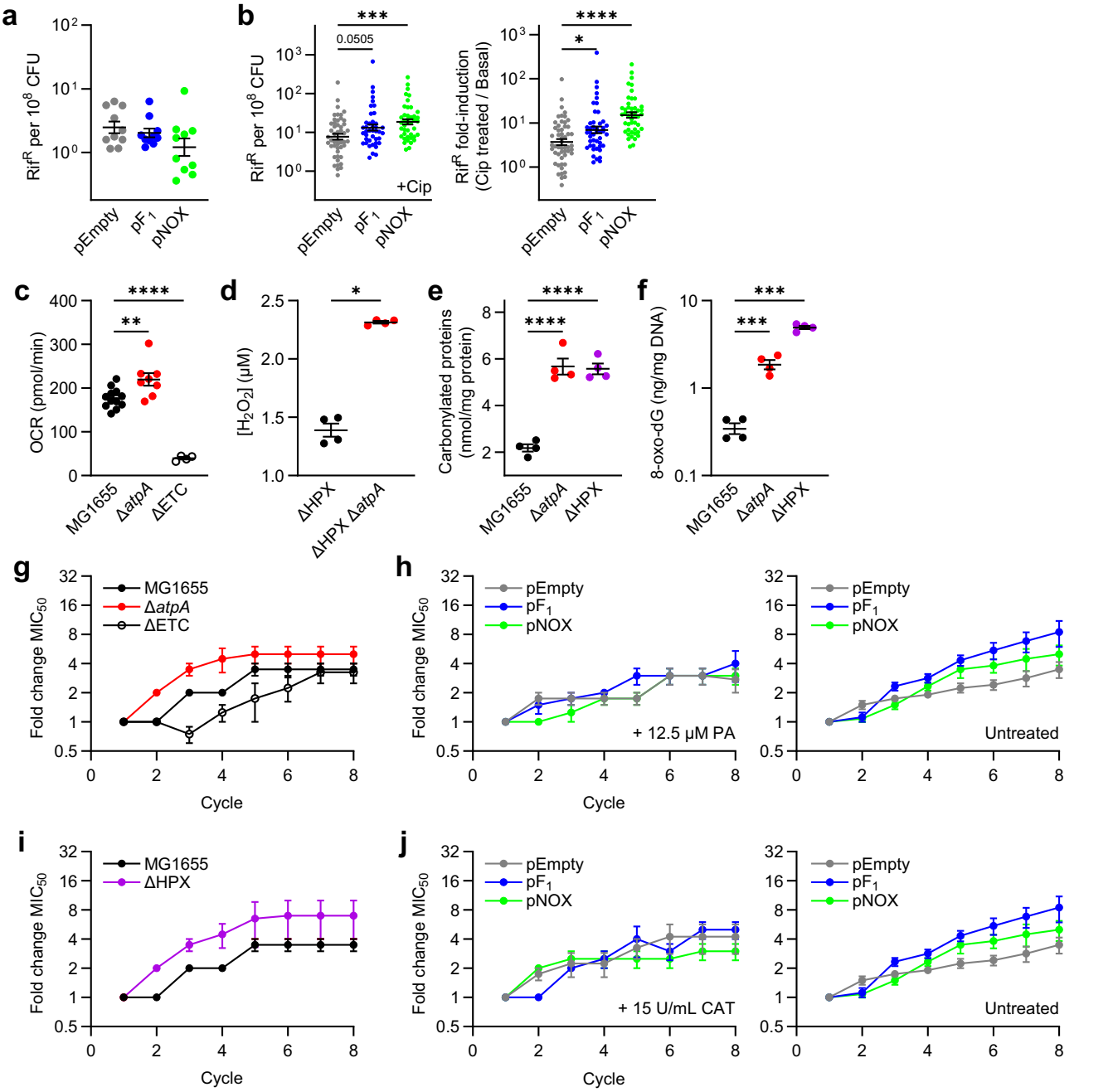

Fig. 3 | Bioenergetic stress accelerates resistance evolution by enhancing ROS production. a Basal mutation rates in pEmpty, pF_1, ($p = 0.8267$) and pNOX ($p = 0.1025$) cells in untreated cells as determined by Luria-Delbrück fluctuation assays[68,69] ($n = 10$). Statistical testing by one-way ANOVA ($p < 0.0001$) with Šídák's multiple comparisons test versus pEmpty. **b** Mutation rates in pEmpty ($n = 48$), pF_1 ($n = 41$; $p = 0.0505$), and pNOX ($n = 42$; $p = 0.0006$) cells following overnight growth in 8 ng/mL ciprofloxacin (Cip) (*left*). Statistical testing by one-way ANOVA ($p = 0.0013$) with Dunnett's multiple comparisons test versus pEmpty. Fold-change in ciprofloxacin-treated mutation rates relative to mutation rates from untreated cells (*right*). Statistical testing by one-way ANOVA ($p < 0.0001$) with Dunnett's multiple comparisons test versus pEmpty (pF_1 $p = 0.0104$, pNOX $p < 0.0001$). **c** Exponential phase oxygen consumption rates (OCR) for wildtype MG1655 ($n = 12$), Δ*atpA* ($n = 8$; $p = 0.0068$), and Δ*cyoA* Δ*cydB* Δ*appB* (ΔETC; $n = 4$; $p < 0.0001$) *E. coli* cells. Statistical testing by one-way ANOVA ($p < 0.0001$) with Dunnett's multiple comparisons test versus MG1655. **d** Integrated H_2O_2 for ΔHPX and ΔHPX Δ*atpA* cells at mid-exponential phase ($OD_{600} \approx 0.5$) ($p = 0.0286$ by two-sided Mann-Whitney test). **e** Carbonylated proteins in exponential phase MG1655, Δ*atpA* ($p < 0.0001$), and ΔHPX ($p < 0.0001$) cells. Statistical testing by one-way ANOVA ($p < 0.0001$) with Dunnett's multiple comparisons test versus MG1655. **f** Oxidized deoxyguanosine in exponential phase MG1655, Δ*atpA* ($p = 0.0002$), and ΔHPX ($p = 0.0001$) cells. Statistical testing by Welch's ANOVA ($p < 0.0001$) with Dunnett's T3 multiple comparisons test versus MG1655. **g** Ciprofloxacin resistance evolution for MG1655, Δ*atpA*, and ΔETC cells. **h** Ciprofloxacin resistance evolution for pEmpty, pF_1, and pNOX cells in the presence (*left*) or absence (*right*) of 12.5 μM respiratory inhibitor piceatannol (PA). Data on untreated cells are replicated from Fig. 1 for comparison. **i** Ciprofloxacin resistance evolution for MG1655 and ΔHPX cells. **j** Ciprofloxacin resistance evolution for pEmpty, pF_1, and pNOX cells in the presence (*left*) or absence (*right*) of 15 μ/mL catalase (CAT). Data on untreated cells are replicated from Fig. 1 for comparison. Data reported as change in the minimum concentration for 50% growth inhibition (MIC_{50}) relative to Cycle 1 for all resistance evolution experiments. All experiments performed in MOPS-rich media. $n = 4$ for all experiments unless otherwise indicated. All data represent biological replicates (independent cultures) and are depicted as mean ± SEM unless otherwise indicated. $^*p \le 0.05$, $^{**}p \le 0.01$, $^{***}p \le 0.001$, $^{****}p \le 0.0001$. $p \ge 0.1$ not shown. Source data are provided within the 'Source Data.xlsx' file.

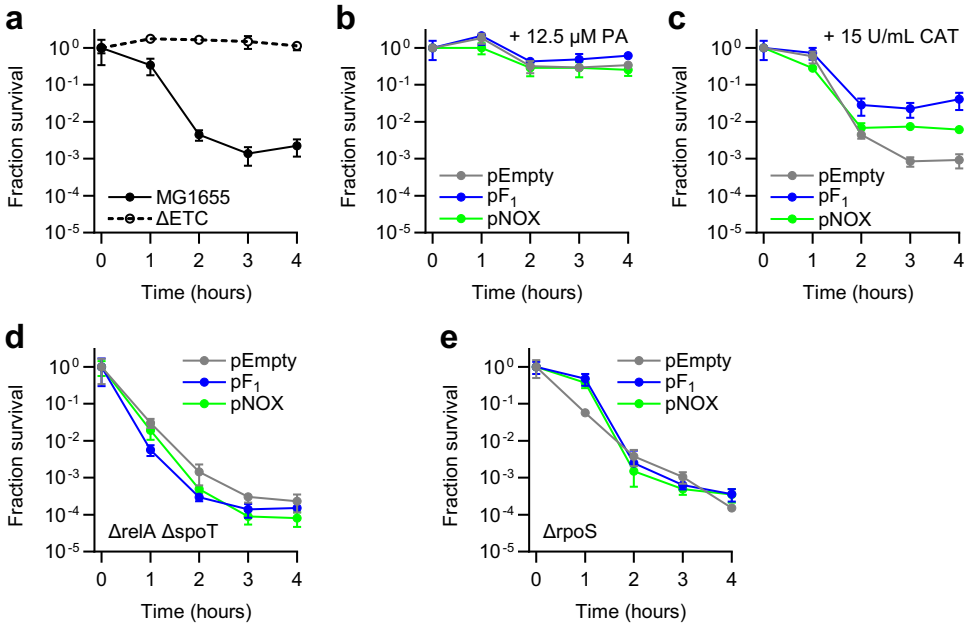

Fig. 4 | Bioenergetic stress potentiates persistence via the stringent response. **a** Ciprofloxacin lethality in wildtype MG1655 and ΔETC cells following treatment with 16 ng/mL ciprofloxacin. **b** Ciprofloxacin lethality in pEmpty, pF_1, and pNOX cells following treatment with 18 ng/mL ciprofloxacin and 12.5 μM piceatannol (PA). **c** Ciprofloxacin lethality in pEmpty, pF_1, and pNOX cells following treatment with 18 ng/mL ciprofloxacin and 15 μ/mL catalase (CAT). **d** Ciprofloxacin lethality in Δ*relA ΔspoT* cells expressing pEmpty, pF_1, or pNOX following treatment with 18 ng/mL. **e** Ciprofloxacin lethality in Δ*rpoS* cells expressing pEmpty, pF_1, or pNOX following treatment with 18 ng/mL ciprofloxacin. Data reported as change in colony-forming units (CFUs) relative to time 0 for all time-kill experiments. Data represent biological replicates (independent cultures) and are depicted as mean ± 95% CI. All experiments performed in MOPS-rich media. $n = 4$ for all experiments. Source data are provided within the 'Source Data.xlsx' file.

resistance, was caused by increased respiration and ROS, we performed time-kill experiments in the presence or absence of supplemented piceatannol or catalase. Similar to low-respiring ΔETC cells (Fig. 4a), respiratory inhibition by piceatannol inhibited ciprofloxacin lethality (Fig. 4b and Supplementary Fig. 5a)[26]. ROS detoxification by catalase did not prevent the increased persistence observed in pF_1 or pNOX cells (Fig. 4c), with persistence levels similar to untreated conditions (Supplementary Fig. 5b). These results indicated that bioenergetic stress-enhanced resistance and persistence were caused by different mechanisms.

Persister cell formation frequently involves activation of the (p)ppGpp-mediated stringent response. This general stress response responds to and protects against diverse stressors by inducing growth inhibition and metabolic dormancy[74]. Stringent response activation involves the synthesis of the alarmone (p)ppGpp by the pyrophosphokinase RelA and the bifunctional (p)ppGpp synthetase/hydrolase SpoT. (p)ppGpp binds and activates the transcription factor DksA, inducing several pleiotropic effects, including activation of the general stress response sigma factor RpoS. To determine if bioenergetic stress potentiates persistence by enhancing stringent response activity, we performed time-kill experiments in Δ*relA ΔspoT* (Fig. 4d) and Δ*rpoS* (Fig. 4e) cells expressing pF_1, pNOX, or pEmpty. These experiments revealed no differences in persistence between pEmpty and pF_1 or pNOX cells, mechanistically implicating the involvement of the stringent response in bioenergetic stress-enhanced persistence.

Persister cell formation can be either environmentally triggered or pre-existing in a population (spontaneously formed during exponential growth)[7,75]. To determine whether bioenergetic stress enhanced persistence by increasing the fraction of pre-existing persister cells, we performed fluorometric assays for stringent response activity in pF_1, pNOX, and pEmpty cells. First, we assayed intracellular (p)ppGpp accumulation by fluorescence microscopy using the genetically encoded S2 (p)ppGpp fluorescent biosensor[76]. S2 is an RNA-based biosensor that is comprised of a (p)ppGpp-specific aptamer and an inactive fluorogenic aptamer (Broccoli[77]). Upon (p)ppGpp binding, Broccoli is activated and fluoresces in the presence of its cognate dye DFHBI-1T. We transformed S2-expressing cells with the pF_1, pNOX, and pEmpty plasmids and verified that S2 fluorescence was higher in stationary phase pEmpty cells than in exponential phase cells (Supplementary Fig. 6a). We imaged exponential phase S2 pF_1 and S2 pNOX cells (>300 cells per strain) and did not find enhanced fluorescence in pF_1 or pNOX cells relative to pEmpty cells (Supplementary Fig. 6b). These suggested that bioenergetic stress alone did not enhance basal intracellular (p)ppGpp accumulation.

Our initial time-kill experiments suggested that persister cells only comprised 0.1-1% of the total population of exponential phase cells in our system (Fig. 1h). Thus, it was possible that our fluorescence microscopy experiments lacked statistical sensitivity to detect changes in the abundance of persister cells. We therefore performed flow cytometry analyses using strains possessing the chromosomally integrated stringent response reporters RpoS::mCherry[78] or rmfp::mCherry[11] that were expressing the pF_1, pNOX, or pEmpty plasmids (>90,000 cells per strain). We found that during exponential phase, the fraction of mCherry-positive pF_1 or pNOX cells did not exceed the fraction of mCherry-positive pEmpty cells for either reporter (Supplementary Fig. 6c, d). These corroborate our S2 microscopy experiments. Interestingly, the fraction of mCherry-positive pF_1 and pNOX cells was significantly higher than the fraction of mCherry-positive pEmpty cells during the stationary phase (Supplementary Fig. 6e, f). These supported our observations that pF_1 and pNOX cells possessed longer lag phases than pEmpty cells (Fig. 1d). Together, these data reveal that bioenergetic stress alone does not enhance persistence by increasing the fraction of pre-existing persister cells.

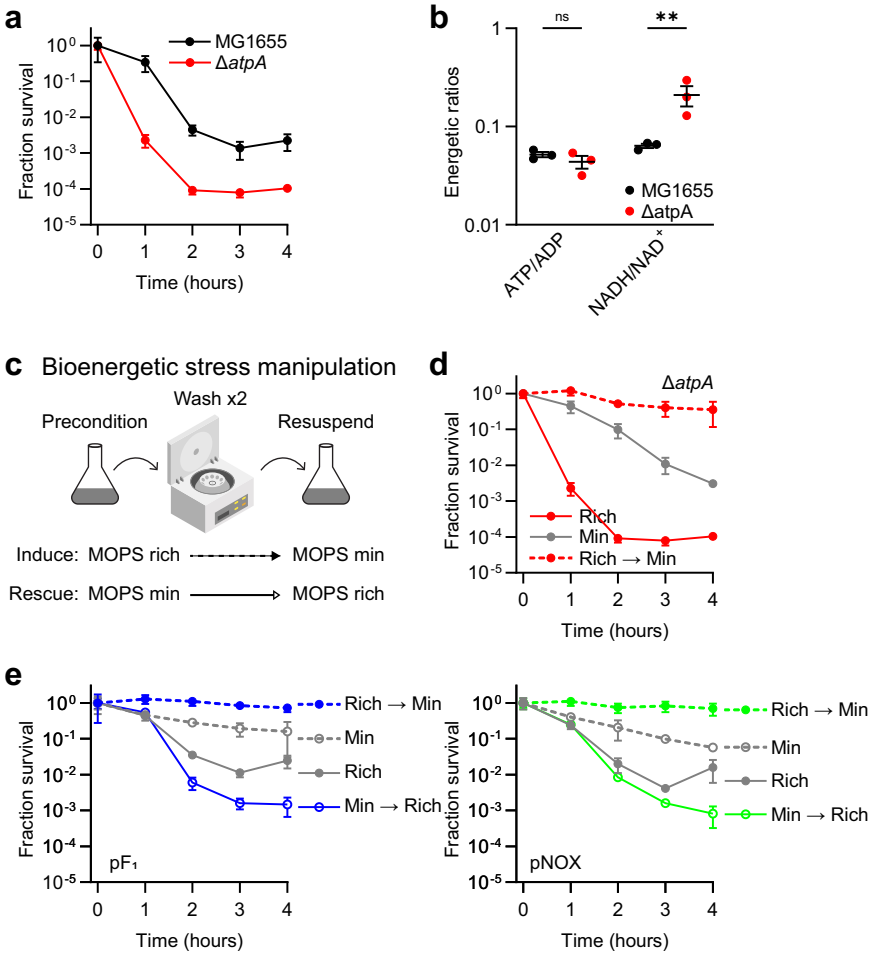

Fig. 5 | Bioenergetic stress is needed for enhanced persistence in highly respiring cells. a Ciprofloxacin lethality in wildtype MG1655 and Δ*atpA* cells following treatment with 16 ng/mL ciprofloxacin in MOPS-rich media. **b** Energetic ratios for exponential phase MG1655 and Δ*atpA* cells grown in MOPS minimal media ($n = 3$ independent cultures, biological replicates) ($p = 0.3182$ for ATP/ADP and 0.0097 for NADH/NAD+ by two-sided unpaired t test). **c** Schematic for bioenergetic stress manipulation by media switching. Cells were bioenergetically preconditioned by growth to the exponential phase in MOPS-rich or minimal media. Exponential phase cells were washed twice in the target working media (rich or minimal media) and then resuspended in rich or minimal media containing ciprofloxacin. Cultures were sampled hourly and plated for CFU enumeration after media switching. Bioenergetic stress is induced by resuspending cells preconditioned in rich media into minimal media. Bioenergetic stress is rescued by resuspending cells preconditioned in minimal media into rich media. **d** Ciprofloxacin lethality in Δ*atpA* cells grown and treated with 16 ng/mL ciprofloxacin in rich media, minimal media, or following a switch from rich media to minimal media. Bioenergetic stress induction enhances persistence in Δ*atpA* cells. **e** Ciprofloxacin lethality in pF_1 or pNOX cells grown and treated with 18 ng/mL ciprofloxacin in rich media, minimal media, following a switch from rich media to minimal media, or following a switch from minimal media to rich media. Rescue of bioenergetic stress decreases persistence in pF_1 and pNOX cells. Data reported as change in colony-forming units (CFUs) relative to time 0 for all time-kill experiments. $n = 4$ for all experiments unless otherwise indicated. Data represent biological replicates (independent cultures) and are depicted as mean ± 95% CI for all time-kill experiments. ns > 0.05, $^{**}p \leq 0.01$. Source data are provided within the 'Source Data.xlsx' file.

Bioenergetic stress is needed for enhanced persistence in highly respiring cells

Our findings that persistence is increased in high-respiring pF_1 and pNOX cells seemingly contradicted our previous findings that increased respiration enhances antibiotic killing[26]. Like bioenergetically stressed pF_1 and pNOX cells, high-respiring Δ*atpA* cells exhibited fitness defects, increased respiration, increased glycolytic activity, and increased ROS accumulation (Fig. 3c–f and Supplementary Figs. 4a and 7a, b). However, Δ*atpA* cells possessed faster lethality and lower persistence than wild-type cells (Fig. 5a). Due to these metabolic similarities, we hypothesized that Δ*atpA* cells would also be bioenergetically stressed. To test this hypothesis, we metabolically profiled Δ*atpA* cells by LC-MS/MS and surprisingly did not observe decreased ATP/ADP or NADH/NAD^+ relative to wildtype cells (Fig. 5b, Supplementary Fig. 7c, d, and Supplementary Data 7). However, like pF_1 and pNOX cells, we observed increased accumulation of central carbon metabolites (acetyl-CoA, citrate, fumarate, succinate, pyruvate). These indicated that Δ*atpA* cells were not bioenergetically stressed. Thus, this provided us with a genetic model that decoupled the physiological effects of bioenergetic stress from the metabolic effects of bioenergetic stress.

We hypothesized that bioenergetic stress was specifically required for enhanced persistence in highly respiring cells. To test this hypothesis, we developed an assay to manipulate bioenergetic stress by rapidly switching cells between rich and minimal media at the moment of antibiotic treatment (Fig. 5c). The rationale for this assay is as follows. In non-stressed cells (homeostatic conditions), energetic equilibrium is established by matching ATP production to ATP consumption[79,80]. Because ATP-consuming anabolic processes (necessarily) correlate with growth rate, ATP consumption and production are higher during growth in rich media than in minimal media[81]. Therefore, we expect a rapid switch from rich to minimal media to induce bioenergetic stress by causing ATP consumption to acutely exceed ATP production. Similarly, we expect a rapid switch

from minimal to rich media to alleviate (rescue) bioenergetic stress by causing ATP production to acutely exceed ATP consumption. We hypothesize that imbalances between ATP consumption versus production are created by the lag in proteome remodeling following a sudden shift in anabolic demand, analogous to the lag phase observed during diauxic growth[82].

We performed time-kill experiments in Δ*atpA* cells, where exponential-phase cells grown in rich media were rapidly switched to minimal media containing ciprofloxacin. We found that bioenergetically stressed Δ*atpA* cells were significantly protected from ciprofloxacin (Fig. 5d). This suggested that the onset of bioenergetic stress during antibiotic treatment was sufficient for causing increased persistence. Importantly, this protection exceeded the level of lethality observed in Δ*atpA* cells only grown and treated in minimal media, where ATP consumption and production are both expected to be low. Thus, this protection was not only explained by slower killing in a poorer nutrient environment.

We next sought to determine if bioenergetic stress was necessary for the enhanced persistence in pF_1 and pNOX cells. We performed time-kill experiments in pF_1 and pNOX cells, where exponential phase cells grown in minimal media were rapidly switched to rich media containing ciprofloxacin. We found that bioenergetically rescued cells were sensitized to ciprofloxacin lethality (Fig. 5e) to levels like pEmpty cells grown and treated in rich media (Fig. 1h). Importantly, this potentiated lethality exceeded the level of lethality observed in pF_1 and pNOX cells grown and treated in rich media where ATP consumption and production are both expected to be high. Conversely, pF_1 and pNOX cells grown in rich media and treated in minimal media exhibited less killing than cells grown and treated in either rich or minimal media alone (Fig. 5e). Because pF_1, pNOX, and Δ*atpA* cells convergently exhibit metabolic enhancements to respiration and ROS production, but exhibit opposite effects persistence phenotypes relative to their respective controls, and because Δ*atpA* cells do not experience bioenergetic stress (Fig. 5b), these results revealed that the physiological consequences of bioenergetic stress are a stronger determinant of antibiotic lethality and persistence than their metabolic consequences alone.

Bioenergetic stress accelerates resistance evolution via "gambler cell" formation and transcription-coupled repair

We next sought to understand the DNA repair mechanisms underlying bioenergetic stress-enhanced resistance evolution. Two mechanisms were recently proposed for ROS-enhanced ciprofloxacin resistance evolution. Rosenberg et al. proposed that ROS potentiate resistance evolution by enabling the formation of a subpopulation of hypermutagenic "gambler cells"[10,11]. In this model, ciprofloxacin- and ROS-induced[83] double-strand DNA breaks activate the SOS response. This initiates a cascade of events involving enhanced ROS accumulation, stringent response activation, and the formation of a *rpoS*-high subpopulation of cells with upregulated expression of low-fidelity translesion DNA polymerases (Pols IV, V, and II). Mutations are introduced by these low-fidelity polymerases during mutagenic break repair[84]. Merrikh et al. proposed that ROS potentiate resistance evolution via transcription-coupled repair[15,16]. In this model, oxidative DNA lesions induce the accumulation of stalled RNA polymerases, which recruit the DNA translocase Mfd to initiate mutagenic nucleotide excision repair via the UvrABC complex. Mutations are spontaneously formed by uncorrected errors in DNA synthesis introduced by Pol I[85].

To test the involvement of gambler cells, we performed resistance evolution experiments in *ΔrelA ΔspoT* (stringent response-deficient), *ΔdinB* (Pol IV-deficient), and *ΔumuD* (Pol V-deficient) cells expressing pF_1, pNOX, or pEmpty. We did not detect statistically significant differences in resistance evolution between pEmpty and pF_1 or pNOX cells in any of these genetic backgrounds (Fig. 6a–c and Supplementary Fig. 8a–d). However, resistance evolution in Δ*relA ΔspoT* cells appeared modestly accelerated relative to wildtype cells and resistance evolution in Δ*relA ΔspoT* pNOX cells appeared modestly accelerated relative to pEmpty cells for reasons unclear. Interestingly, there did not seem to be an effect on resistance evolution between wild-type pEmpty cells and Δ*dinB* or Δ*umuD* cells, suggesting that these DNA repair mechanisms act to enhance bioenergetic stress-induced evolution and not basal evolution. Because Δ*relA ΔspoT* cells are unable to induce the stringent response, they cannot form a hyper-mutagenic subpopulation[11]. Together, these results support the hypothesis that bioenergetic stress accelerates resistance evolution by potentiating gambler cell formation.

To test the involvement of transcription-coupled repair, we performed ciprofloxacin resistance evolution experiments in *Δmfd* cells expressing pF_1, pNOX, or pEmpty. We also did not find statistically significant differences in resistance evolution between these cells (Fig. 6e and Supplementary Fig. 8e). Moreover, our RNA sequencing data revealed modestly increased *uvrB* expression in pF_1 and pNOX cells over pEmpty cells and modestly increased *mfd* expression in pNOX cells over pEmpty cells (Fig. 6f and Supplementary Data 5). Thus, these results also support the hypothesis that bioenergetic stress accelerates resistance evolution via transcription-coupled repair.

Discussion

Our findings here reveal several unexpected and important insights into how intrinsic bioenergetic stress impacts antimicrobial resistance, persistence, and bacterial physiology (Fig. 7). Despite commonly held notions that protection from antimicrobial stress involves metabolic dormancy[5,8,40–45], our data demonstrate that metabolic quiescence is not required for persistence. Thus, our data enrich existing paradigms that associate hyper-metabolic activity and ROS with antibiotic lethality[13,14,26,27,46,47,83,86,87]; we discovered that populations with high metabolic activity and ROS production can unexpectedly become enriched for persister cells. Our data suggest that the bioenergetic balance between ATP consumption versus production (indexed by the ATP/ADP ratio or AEC) is a key metabolic determinant of persister cell formation, even in hypermetabolic cells.

Our data seemingly contradict findings in another study that proposed that ATP depletion itself does not cause persistence[88,89]. In that study, the authors observed enhanced persistence in *Salmonella* cells expressing an IPTG-inducible *atpAGD* plasmid and speculated that the enhanced persistence was caused by slow growth. However, our pF_1 cells exhibited enhanced persistence without significant growth rate defects (Fig. 1b). Moreover, we observed enhanced killing in Δ*atpA* cells, which exhibited slow growth (Supplementary Fig. 7a). The authors also showed that the bacteriostatic protein translation inhibitor chloramphenicol significantly increased intracellular ATP while inhibiting ciprofloxacin lethality. Thus, the authors concluded that persistence is determined by defective growth rates/processes and not ATP availability. Their findings are consistent with our previous work[23], but we posit that chloramphenicol's inhibition of fluoroquinolone lethality is not caused by growth arrest. Our previous work revealed that chloramphenicol interrupts fluoroquinolone lethality by attenuating cellular respiration at time points when growth is ill-defined[23]. Moreover, others showed that chloramphenicol can inhibit fluoroquinolone lethality by preventing the release of broken DNA from gyrase[90]. In addition, our media-switching experiments here reveal that persistence is not fully determined by pre- or post-treatment conditions associated with high or low growth rates (in rich versus minimal media) (Fig. 5).

Instead, we propose a model in which antibiotic lethality and persistence are determined by the relative rates of ATP consumption versus production instead of only the concentration of intracellular ATP. Our model predicts that antibiotic lethality is higher when equilibrated ATP consumption and production rates are both high (e.g., during exponential growth) than when these rates are both low (e.g.,

https://doi.org/10.1038/s41467-025-60302-6

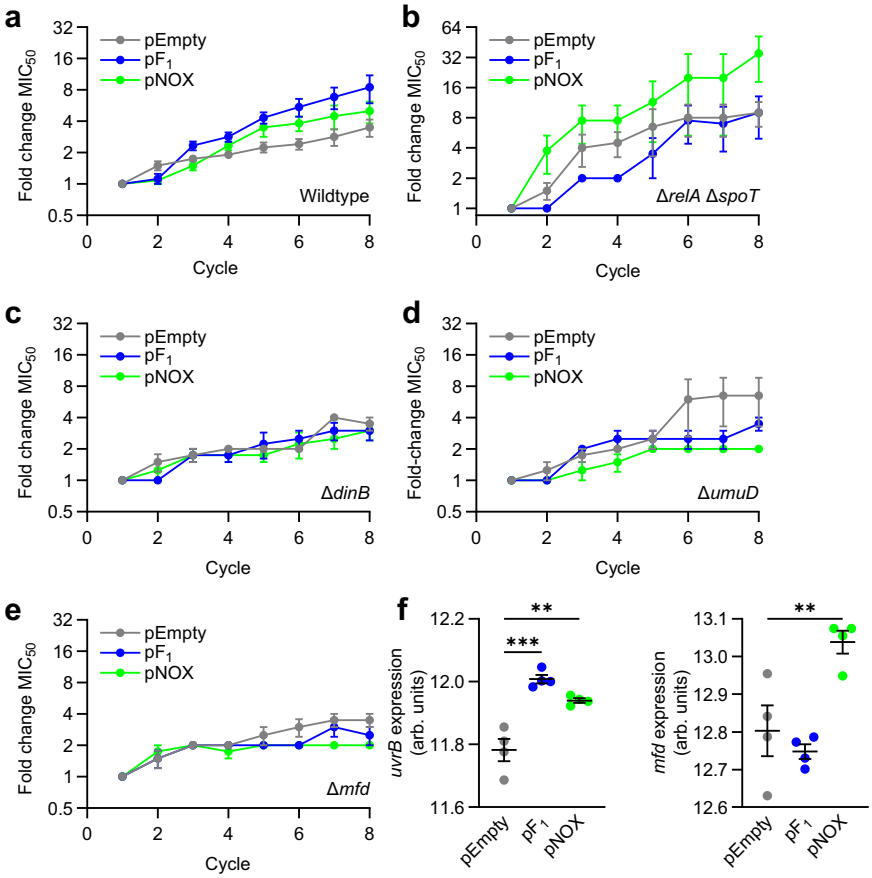

Fig. 6 | Bioenergetic stress accelerates resistance evolution via "gambler cell" formation and transcription-coupled repair. a Ciprofloxacin resistance evolution for wildtype MG1655 cells expressing pEmpty, pF_1, or pNOX. These data are replicated from Fig. 1 to facilitate comparisons. **b** Ciprofloxacin resistance evolution for *ΔrelA ΔspoT* cells expressing pEmpty, pF_1, or pNOX. **c** Ciprofloxacin resistance evolution for *ΔdinB* cells expressing pEmpty, pF_1, or pNOX. **d** Ciprofloxacin resistance evolution for *ΔumuD* cells expressing pEmpty, pF_1, or pNOX. **e** Ciprofloxacin resistance evolution for *Δmfd* cells expressing pEmpty, pF_1, or pNOX. Data reported as change in the minimum concentration for 50% growth inhibition (MIC_{50}) relative to Cycle 1 for all resistance evolution experiments. **f** *uvrA* (*left*) and *mfd* (*right*) expression for exponential phase pEmpty, pF_1, and pNOX cells. Data depicted as quantile-normalized log_2-transformed transcripts per million counts as measured by RNA-sequencing. Statistical testing by one-way ANOVA with Dunnett's multiple comparisons test versus pEmpty for *uvrA* ($p = 0.0002$; pF_1 $p = 0.0001$, pNOX $p = 0.0014$) and *mfd* ($p = 0.0027$; pF_1 $p = 0.5940$, pNOX $p = 0.0082$). All experiments performed in MOPS-rich media. $n = 4$ for all experiments. All data represent biological replicates (independent cultures) and are depicted as mean ± SEM. $^{**}p \le 0.01$, $^{***}p \le 0.001$. Non-significant comparisons not shown. Source data are provided within the 'Source Data.xlsx' file.

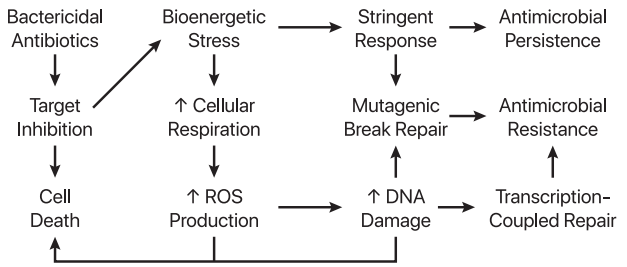

Fig. 7 | Antibiotic-induced bioenergetic stress potentiates antimicrobial resistance and persistence. Antibiotic treatment induces bioenergetic stress by increasing ATP consumption[21,23]. Bioenergetic stress increases cellular respiration and ROS production. Increased ROS accelerates resistance evolution by mutagenic break repair and transcription-coupled repair. Bioenergetic stress potentiates antimicrobial persistence via the stringent response. Stringent response activation enables resistance evolution by mutagenic break repair.

during the stationary phase). Our model also predicts that if ATP consumption significantly increases before ATP production can increase to meet demand, and/or if ATP production rapidly decreases (e.g., under nutrient starvation[28]), bioenergetic stress increases and antibiotic lethality decreases via the stringent response (Fig. 5d). Conversely, if ATP consumption rapidly decreases, and/or if ATP production rapidly increases (e.g., by directly stimulating oxidative phosphorylation[87]), bioenergetic stress decreases and antibiotic lethality increases (Fig. 5e). This model is supported by observations that diauxic shifts stimulate persister cell formation[91], as a diauxic shift is expected to rapidly decrease ATP production before the proteome can remodel. This model also predicts that bacteriostatic antibiotics will antagonize bactericidal antibiotics[92], as bacteriostatic antibiotics decrease both ATP consumption and ATP production[26]. Because antibiotic treatment itself induces bioenergetic stress (Fig. 1a), our model predicts a zone of antibiotic efficacy for bactericidal antibiotics: at moderate antibiotic treatment concentrations, enhanced ATP consumption induces compensatory hypermetabolic ATP production that enhances lethality[24,25]; while at very high antibiotic concentrations, our model predicts that ATP production is unable to meet the enhanced demand for ATP and lethality is decreased as a consequence of the increased bioenergetic stress. This prediction is consistent with the Eagle effect, in which antibiotic lethality is paradoxically decreased at high antibiotic treatment concentrations for some antibiotics in many microorganisms[93–95]. However, this may not be universal to all bactericidal antibiotics or all bacteria and remains to be directly investigated.

Our work here implicates the stringent response in bioenergetic stress-enhanced persistence (Figs. 4d, e). Importantly, our model does not exclude mechanisms of bioenergetic stress-enhanced persistence, such as decreased antibiotic target activity[42] or altered drug transport[96]. These might be expected to be downstream of stringent response activation. However, the molecular details for how cells sense bioenergetic stress and induce the stringent response are unclear. The (p)ppGpp synthetases RelA and SpoT are specifically activated only by uncharged tRNAs or acyl carrier proteins, respectively[74]. Protein synthesis is the most ATP-consuming process in bacterial cell replication[81], for which tRNA charging is the only step that directly consumes ATP. Thus, it is possible that charged tRNAs are depleted under bioenergetic stress, thus activating RelA. Alternatively, our RNA sequencing data revealed that acyl carrier protein (*acpP*) gene expression decreased ~15–20% in both pF_1 and pNOX cells relative to pEmpty cells (Supplementary Data 3). Moreover, our metabolic modeling analyses predicted that the activities of several fatty acid and cell wall synthesis reactions are decreased in both pF_1 and pNOX cells. Thus, it is also possible that acyl carrier proteins are depleted under bioenergetic stress, thus activating SpoT. Both these hypotheses remain untested.

In this work, we show that intrinsic bioenergetic stress can itself potentiate mutagenesis. Our work reveals that imbalanced ATP consumption and production enhance mutagenesis by stimulating bacterial metabolism and ROS production. Importantly, this potentiation only occurs for stress-induced mutagenesis and not basal mutagenesis. While ROS-induced mutagenesis is well-studied[39], several questions remain on the molecular events linking bioenergetic stress to increased mutation rates. Our data suggest both mutagenic break repair[10,11] and transcription-coupled repair[15,16] are involved in bioenergetic stress-enhanced resistance evolution. Our findings that bioenergetic stress-potentiated ciprofloxacin resistance evolution is curbed in Δ*relA ΔspoT* cells is consistent with findings by others that the stringent response is involved in antimicrobial resistance evolution[97–102]. Thus, our data also support the hypothesis that antibiotic persistence facilitates resistance evolution[9,12] by providing a reservoir of hyper-mutagenic "gambler cells"[11]. However, other mutagenic DNA repair mechanisms are possibly involved. Such mechanisms include base-excision repair[103] and mismatch repair[104] pathways, which participate in ROS-induced mutagenesis. Understanding these molecular mechanisms will enable the exciting development of anti-evolution drug adjuvants that can prevent or curb the expansion of drug-resistant infections[16–20,105].

Our findings have important implications for the therapeutic management of bacterial infections. Our results suggest that antimicrobial treatment enhances persister cell formation via bioenergetic stress-mediated induction of the stringent response. This enriches our understanding of why antibiotic cross-resistance is prevalent for many classes of antimicrobial agents[106–108] and disinfectants[109,110] for diverse pathogens, although other mechanisms may be relevant as well. Moreover, many stresses associated with bacterial biofilms or innate immune cell phagolysosomes can induce bioenergetic stress, including hypoxia[30], oxidative stress[31], and acid stress[32]. This notion complements our previous findings that the actions of antibiotics on host cells present at the site of infection can augment antibiotic efficacy[111]. Thus, our data suggest that the host environment of infection may also play a key role in driving antimicrobial resistance and persistence[112]. This is particularly relevant for diseases such as tuberculosis, where resistance is only acquired by de novo mutations[3], and the innate immune response to infection induces hypoxic granuloma formation and phagocytic internalization of *Mycobacterium tuberculosis* cells[113,114]. However, we performed this study in an *E. coli* laboratory strain, and it remains to be investigated how generalizable our findings will be to other bacteria.

Finally, our findings have several implications for research domains beyond antimicrobial resistance and infectious disease. For example, the bioenergetic stress created by heterologous gene and protein expression limits productive yield in metabolic engineering applications[33] and gene circuit failure in synthetic biology applications[115,116]. Mechanistically understanding the physiological responses to bioenergetic stress can enable interventions that increase ATP production, decrease ATP consumption, and/or inhibit the adverse consequences of bioenergetic stress to enhance the productive yield of bioreactors[117] and the genetic stability of synthetic gene circuits[118]. Indeed, because bioenergetic metabolites such as ATP and NADH are universally essential cofactors across the tree of life[54], much is to be explored in understanding the mechanisms and physiological consequences of bioenergetic stress.

Methods

Bacterial strains, media, growth conditions, and chemical reagents

All experiments were performed in *Escherichia coli*. Strains used in this study were wildtype MG1655, MG1655 Δ*cheY*, MG1655 Δ*flhD*, MG1655 Δ*ahpCF* Δ*katE* Δ*katG* (ΔHPX), MG1655 Δ*atpA*, ΔHPX Δ*atpA*, MG1655 Δ*cyoA* Δ*cydB* Δ*appB* (ΔETC), MG1655 Δ*dinB*, MG1655 Δ*mfd*, MG1655 Δ*umuD* MG1655 Δ*relA* Δ*spoT*::kan^R, MG1655 Δ*rpoS*, and pET-28c-S2 expressing BL21(DE3) strains expressing pEmpty, pF_1, or pNOX. Details on strains used in this study are provided in Supplementary Data 8.

Unless otherwise specified, cells were cultured in MOPS EZ rich defined media (#M2105 Teknova; Hollister, CA). For cloning, cells were cultured in Luria-Bertani (LB) broth (#244620 Becton Dickinson; Franklin Lakes, NJ). For metabolomics experiments, cells were cultured in MOPS EZ minimal media (#M2106 Teknova). Cells were grown at 37 °C in baffled flasks or 14 mL test tubes with 300 rpm shaking, in round-bottom 96-well plates with 900 rpm shaking, or in an Infinite M Plex plate reader (Tecan; Mannedorf, Switzerland) with 900 rpm shaking.

All antibiotics and chemical reagents were purchased from Sigma-Aldrich (St. Louis, MO) unless otherwise specified. Uniformly labeled ^{13}C glucose was purchased from Cambridge Isotope Laboratories (#CLM-1396, Tewksbury, MA). Strains with antibiotic selection markers were grown in media containing 30 μg/mL chloramphenicol, 100 μg/mL ampicillin, or 50 μg/mL kanamycin. All experiments were performed with $n \geq 3$ from independent overnight cultures starting from single colonies on LB agar plates (#244520 Becton Dickinson).

Gene knockout strain construction

MG1655 Δ*atpA*, Δ*cheY*, Δ*dinB*, Δ*flhD*, Δ*mfd*, Δ*umuD*, and Δ*rpoS* strains were constructed by P1 phage transduction using the Keio collection[119], as described previously[21]. Briefly, overnight cultures of *E. coli* BW25113 kan^R cells grown in LB media were inoculated 1:100 into fresh media supplemented with 0.2% glucose and 5 mM $CaCl_2$ and allowed to grow for 1 h before P1 phage was added. After 2 h of incubation, phage lysates were passed through a 0.22 μm filter to remove the remaining bacteria. An overnight culture of MG1655 was pelleted by centrifugation at 4200 x *g* for 10 min and resuspended in a 10 mM $MgCl_2$ and 5 mM $CaCl_2$ salt solution, then incubated with the phage lysate at 37 °C for 30 min. LB containing 5 mM sodium citrate was added to each tube and incubated at 37 °C for an additional 60 min in a 300 rpm shaking incubator. Cells were pelleted by centrifugation at 6000 x *g* for 2 min, resuspended in fresh media containing 5 mM sodium citrate, and then plated on kanamycin-selective LB agar plates containing 5 mM sodium citrate. After 24 h of incubation, colonies were selected from each plate, and their kanamycin-resistance cassettes were cured by transforming the pCP20 plasmid[120] via electroporation, inducing recombination by overnight growth at 42 °C, and then screening resulting colonies for genomic recombination and plasmid loss on kanamycin- and ampicillin-selective LB agar plates. ΔHPX was constructed by curing the kanamycin-resistance cassette from MG1655 Δ*ahpCF* Δ*katE*::kan^R Δ*katG* by pCP20 as described above. ΔHPX Δ*atpA* was

constructed by P1 phage transduction of Δ*atpA*::kan^R into ΔHPX and curing the kanamycin-resistance cassette as described above.

Plasmid generation

The plasmid backbone shared by pEmpty, pF_1, and pNOX consists of a p15 origin of replication, chloramphenicol resistance, and a constitutive synthetic promoter derived from pAB191:lacZ[121]. pEmpty was generated by PCR amplification and restriction cloning of the plasmid backbone without the lacZ gene insert. pF_1 was generated by PCR amplification of *atpAGD* from *E. coli* MG1655, PCR amplification of the synthetic promoter from pCP41::atpAGD plasmid[35,36], and by restriction cloning of these fragments into pEmpty. pNOX was generated by PCR amplification of the fragment containing the synthetic promoter and *Streptococcus pneumoniae* NADH oxidase from the pAC06::nox plasmid[36] and by restriction cloning into pEmpty. All constructs were fully sequenced for validation. Plasmid maps are available on request.

Metabolomic characterization

Intracellular metabolites from ciprofloxacin-treated or untreated *E. coli* cells were extracted and quantified on an AB SCIEX Qtrap 5500 mass spectrometer (AB SCIEX; Framingham, MA) with a Prominence UFLC XR HPLC (Shimadzu; Columbia, MD) using an ACQUITY UPLC HSS T3 Column (100 Å, 1.8 μm, 2.1 mm X 30 mm) (Waters; Milford, MA) as described previously[48,122]. Solvent A was comprised of 10 mM tributylamine, 10 mM acetic acid (pH 6.86), 5% methanol, and 2% 2-propanol. 2-propanol was used for Solvent B.

Intracellular metabolites from untreated pEmpty, pF_1, and pNOX cells were extracted and quantified on an Orbitrap IQ-X Tribid mass spectrometer with a coupled Vanquish Horizon UHPLC system (Thermo Scientific; Waltham, MA) using an XBridge BEH Amide column (2.5 μm, 2.1 mm X 150 mm) (Waters; Milford, MA) as described previously[123]. Solvent A was comprised of 95:5 H_2O:acetonitrile with 20 mM acetic acid, 40 mM ammonium hydroxide, pH 9.4. Solvent B was comprised of 20:80 H_2O:acetonitrile with 20 mM acetic acid, 40 mM ammonium hydroxide, pH 9.4.

Intracellular metabolites from untreated MG1655 and Δ*atpA* cells were extracted and quantified on an Orbitrap Q Exactive mass spectrometer with a coupled Vanquish UHPLC system (Thermo Scientific) using an XBridge BEH Amide column as described previously[123]. Solvent A was comprised of 95:5 H_2O:acetonitrile with 20 mM acetic acid, 40 mM ammonium hydroxide, pH 9.4. Solvent B was comprised of 20:80 H_2O:acetonitrile with 20 mM acetic acid, 40 mM ammonium hydroxide, pH 9.4.

For each set of samples, overnight cultures grown in MOPS minimal media were inoculated 1:500 into fresh media and grown until they reached $OD_{600} \geq 0.1$. For experiments involving ciprofloxacin treatment, cells were back-diluted to $OD_{600} = 0.1$ in 25 mL MOPS minimal media, dispensed into 250 mL baffled flasks, and treated with 16 ng/mL ciprofloxacin or solvent control (H_2O) for 1 h before extraction. Aliquots with biomass equivalents to 10 mL of cell culture at $OD_{600} = 0.1$ were collected and immediately subjected to metabolite extraction using a 40:40:20 mixture of acetonitrile, methanol, and LC-MS grade water pre-chilled to −20 °C and maintained on dry ice as described previously[124]. Samples were rapidly collected by Fast Swinnex filtration in the 40:40:20 extraction solvent and then centrifuged for 5 min at 16,000 rpm at 4 °C. Extracted metabolites were filtered using Phree phospholipid removal filters (#8B-S133-TAK Phenomenex; Torrence, CA). For experiments involving ciprofloxacin treatment, ^{13}C-standards were spiked in during extraction.

Uniformly labeled ^{13}C-standards were generated by growing *E. coli* in uniformly labeled glucose M9 minimal media in baffled flasks[49]. Calibration standards were split across several mixes, aliquoted, and lyophilized to dryness. All samples and calibrators were equally spiked with the same internal standards. Samples were quantified using isotope-dependent mass spectrometry. Calibration curves were run before and after all biological and analytical replicates. The consistency of quantification between calibration curves was checked by running a Quality Control sample composed of all biological replicates.

Full scan data was processed using either AB SCIEX MultiQuant or MAVEN[125]. Raw metabolomics data are provided in Supplementary Data 1, 2, and 7.

NADH and NAD$^+$ quantification

NADH and NAD$^+$ were quantified using the Promega NAD$^+$/NADH-Glo kit (#G9071 Promega; Madison, WI) according to the manufacturer's instructions. Briefly, overnight cultures grown in MOPS-rich media were inoculated 1:500 into fresh media and grown to $OD_{600} \geq 0.2$. Cultures were back-diluted to $OD_{600} = 0.2$, then lysed with 0.1 N NaOH + 0.5% DTAB. For NAD$^+$, 100 μL of lysed cells were treated with 50 μL of 0.4 N HCl and heated to 60 °C for 15 min to decompose NADH, then neutralized with 50 μL of Trizma base. For NADH, 100 μL of lysed cells were heated at 60 °C for 15 min to decompose NAD$^+$, then neutralized with 100 μL of HCl/Trizma solution. Equal volumes of NADH or NAD$^+$ extract and NAD/NADH-Glo Detection Reagent were added to a 96-well flat white plate. After incubating for 1 h, luminescence measurements were taken in a Tecan Infinite M Plex microplate reader. Absolute concentrations of NADH and NAD$^+$ were calculated from a standard curve.

Bacterial growth kinetics

Overnight cultures of cells grown in MOPS-rich were inoculated 1:20,000 into fresh media. 200 μL of diluted cultures were dispensed into 96-well clear round-bottom microplates. Microplates were incubated at 37 °C in a Tecan Infinite M Plex microplate reader at 900 rpm. OD_{600} was measured every 12.5 min for 12 h.

Oxygen consumption and extracellular acidification quantification

Oxygen consumption and extracellular acidification rates were measured using a Seahorse XF^{e}96 Extracellular Flux Analyzer (Agilent; Santa Clara, CA), as described previously[21,25,26]. Briefly, Seahorse XF Pro cell culture microplates were pre-coated with 15 μL 100 μg/mL poly-D-lysine. Overnight cultures grown in MOPS-rich media were inoculated 1:500 into fresh media. Cells were grown until they reached $OD_{600} \geq 0.1$ and then back-diluted to $OD_{600} = 0.0025$. 200 μL of diluted cells were dispensed into coated microplates, and microplates were centrifuged for 10 min at 1500 x *g* to adhere cells. Oxygen consumption rate (OCR) and extracellular acidification rate (ECAR) measurements were made at 4-minute intervals (2.5 min for measurement and 1.5 min for mixing) for 4 cycles. Reported values are derived from 5 technical replicates for each biological replicate. Samples were randomized on each plate to control for potential systematic biases. For experiments involving piceatannol, cells were treated with 12.5 μM piceatannol or 0.5% DMSO after cultures were back-diluted to $OD_{600} = 0.0025$ before measurement.

Minimum inhibitory concentration (MIC) determination

MICs for ciprofloxacin and piceatannol were measured by microbroth dilution; experiments involving ciprofloxacin followed the CLSI standard procedure[55] with the exception that we used MOPS-rich media instead of Mueller-Hinton broth. Ciprofloxacin or piceatannol was serially diluted 1.5-fold in MOPS-rich media at 100 μL volumes in a 96-well round-bottom microplate. The highest working concentration was 40 ng/mL for ciprofloxacin and 100 μg/mL for piceatannol. The last 2 columns of each microplate contained drug-free controls. For ciprofloxacin, overnight cultures grown in MOPS-rich media were inoculated to $OD_{600} = 0.01$, grown to exponential phase ($OD_{600} > 0.3$), then back-diluted to $OD_{600} = 0.0002$. 100 μL of diluted cultures were added to each well of the ciprofloxacin-loaded microplate. For piceatannol, overnight cultures grown in MOPS-rich media were inoculated

1:10,000 into fresh media. 100 µL of diluted cultures were added to each well of the piceatannol-loaded microplate. The last column was not inoculated with cells and used as a cell-free control. Plates were sealed with Breathe-Easy permeable membranes (#Z380059 Sigma-Aldrich) and incubated for 22 h. OD_{600} was measured on a Tecan Infinite M Plex microplate reader.

Resistance evolution

Resistance evolution experiments were performed by serial-dilution passaging. 1 mg/mL stocks of ciprofloxacin were prepared and stored at −20 °C for consistent chemical preparation. Aliquots were thawed and diluted for use in each evolution cycle and were discarded afterward. Ciprofloxacin-loaded microplates were prepared above as in the MIC experiments. Evolution experiments were initiated by growing ancestral *E. coli* cells in MOPS-rich media and inoculating 1:2500 into fresh media. For each cycle, diluted cultures were dispensed into each ciprofloxacin-loaded plate to achieve a final inoculum of 1:5,000 (~1-2·10^6 colony forming units). Plates were sealed with Breathe-Easy permeable membranes and incubated for 22 h. OD_{600} was then measured on a Tecan Infinite M Plex microplate reader. The MIC_{50} was calculated as the concentration of ciprofloxacin required to inhibit growth by ≥50% compared to ciprofloxacin-free growth controls. At each subsequent evolution cycle, the culture from the highest ciprofloxacin concentration in which bacteria grew ($OD_{600} \geq 0.1$) was diluted 1:2500 and re-inoculated into freshly prepared ciprofloxacin-loaded microplates at a volume of 100 µL to achieve 1:5000 final dilution. Bacteria were passaged for a total of 8 cycles. Fold change MIC_{50} was calculated by dividing the MIC_{50} of each cycle by the MIC_{50} of Cycle 1. Areas under the curve were calculated by summing the fold-change MIC_{50}s across all 8 cycles. Cycles to 4 x MIC were determined as the first cycle at which growth was observed at 4 x MIC_{50}. For experiments involving biochemical supplementation, 12.5 µM piceatannol or 15 µ/mL catalase was included in the growth media throughout the entire experiment.

Time-kill kinetics

Ciprofloxacin time-kill experiments were performed as previously described[21]. Briefly, overnight cultures grown in MOPS rich were inoculated 1:500 into fresh media and grown to $OD_{600} \geq 0.1$. Cultures were back-diluted to $OD_{600} = 0.1$ and treated with 16 ng/mL or 18 ng/mL ciprofloxacin as appropriate for achieving ~3-log reduction in survival 4 h post-treatment (Supplementary Fig. 1e). Hourly samples were collected and serially diluted in PBS for colony enumeration 24 h later. High-dose ciprofloxacin, gentamicin, or ampicillin time-kill experiments were performed in the presence of 128 ng/mL ciprofloxacin, 200 ng/mL gentamicin, or 100 µg/mL ampicillin, respectively. Piceatannol or catalase supplementation experiments were performed in the presence of 100 µM piceatannol, 15 µ/mL catalase, or 1% DMSO.

Media switching experiments were performed by preconditioning cells in MOPS-rich or MOPS minimal media, pelleting by centrifugation at 6000 x *g* for 2 min, washing twice in the target working media (MOPS rich or MOPS minimal), and then resuspending in the target working media at $OD_{600} = 0.1$ in the presence of ciprofloxacin.

RNA sequencing and analysis

Overnight cultures grown in MOPS-rich media were inoculated 1:500 into fresh media and grown to $OD_{600} \geq 0.1$. 600 µL cells were then mixed with 1200 µL RNAprotect Bacteria Reagent (#76506 Qiagen; Germantown, MD) to inactivate RNase activity. Total RNA was extracted using RNeasy Micro Kits (#74104 Qiagen). RNA concentrations and RNA integrity were measured on an Agilent 4200 TapeStation. Ribosomal RNA was depleted using the Ribo-Zero Plus rRNA Depletion Kit (#20037135 Illumina; San Diego, CA). cDNA libraries were prepared using the NEBNext Ultra II Directional RNA Library Prep Kit for Illumina (#E7760L, New England Biolabs; Ipswich, MA). RNA sequencing was performed on an Illumina NovaSeq6000 system with 100x coverage.

Raw sequencing reads were aligned to the GenBank U00096.3 NCBI *E. coli* MG1655 reference genome by Bowtie 2[126]. Read counts were compiled using featureCounts[127] and quantile normalized by qsmooth[128]. Data quality, adapter and quality trimming statistics, and alignment and count metrics were compiled and assessed using MultiQC[129]. Differential gene expression analysis was performed using DESeq2[130]. Differentially expressed genes were defined to possess false discovery rate (FDR)-corrected *p*-values ≤ 0.05 and $\log_2$ fold changes ≥ 1 or ≤ −1. Gene Ontology (GO) analyses of differentially expressed genes were performed using PANTHER[131]. FDR correction was performed using the Benjamini-Hochberg method[132]. Normalized sequencing counts, differential expression analyses, GO enrichments, and data for selected genes are provided in Supplementary Datas 3, 4, and 5.

Genome-scale metabolic modeling

Genome-scale metabolic modeling was performed using the iML1515 model of *E. coli* metabolism[63] as described previously[21]. pEmpty cells were modeled using the default iML1515 model. pF_1 cells were modeled by adding an ATP sink reaction (ATPase) defined as "atp_c + h2o_c → adp_c + h_c + pi_c". The lower bound for the ATP sink reaction was assigned to 1.25, which was near the greatest ATP hydrolysis rate that possessed non-zero biomass production. pNOX cells were modeled by adding a NADH oxidase reaction (NOX) defined as "h_c + nadh_c + o2_c → h2o2_c + nad_c". The lower bound for the NADH oxidase reaction was assigned to 1.33, which was near the greatest NADH oxidation rate that possessed non-zero biomass production. Normalized RNA sequencing counts were applied as modeling constraints to iML1515 using the iMAT algorithm[61,62]. Flux sampling was performed using the COBRApy toolbox[133] with 10,000 flux samples collected for each model by optGpSampler[134]. Model simulations are summarized in Supplementary Data 6.

H_2O_2 production

H_2O_2 production was quantified using a highly specific horseradish peroxidase and Amplex UltraRed assay[64]. This assay quantifies H_2O_2 production using ΔHPX cells lacking the ability to scavenge H_2O_2. Intracellular H_2O_2 produced by these cells passively diffuses into and equilibrates within the extracellular medium, which are assayed using horseradish peroxidase (#P8375 Sigma Aldrich) and Amplex UltraRed (#A36006 Thermo Scientific). Overnight cultures grown in MOPS-rich media containing 10 U/mL catalase were inoculated 1:500 into fresh media containing catalase and grown to $OD_{600} \geq 0.1$. Cells were then pelleted by centrifugation at 6000 x *g* for 2.5 min, washed 3 times with fresh media without catalase, and resuspended in fresh media without catalase. Washed cultures were back-diluted to $OD_{600} = 0.05$. 100 µL diluted culture was dispensed into wells of a 96-well black, clear-bottom microplate. A standard curve for H_2O_2 was generated by performing 2-fold serial dilutions at 100 µL volumes. 50 µL of MOPS rich media containing 200 µM Amplex UltraRed was dispensed into each well of the microplate, followed immediately by 50 µL of MOPS rich media containing 100 µg/mL horseradish peroxidase. OD_{600} and fluorescence emissions (550–590 nm) were measured on a Tecan Infinite M-plex microplate reader at 15-minute intervals with 488 nm excitation, and 900 rpm shaking and 37 °C incubation between reads. Absolute H_2O_2 concentrations for each measurement were computed from the standard curve, and H_2O_2 concentrations were normalized to cell density as measured by OD_{600}.

Carbonylated protein quantification

Protein carbonylation was quantified using the OxiSelect Protein Carbonyl ELISA kit (#STA-310 Cell Biolabs; San Diego, CA) according to the manufacturer's instructions, as previously described[135]. Briefly,

overnight cultures grown in MOPS-rich media were inoculated 1:500 into fresh media and grown to $OD_{600} \geq 0.1$. Aliquots with biomass equivalents to 25 mL of cell culture at $OD_{600} = 0.1$ were pelleted by centrifugation at 4250 x *g* for 10 min, washed 3 times with ice-cold PBS, flash frozen, and stored at − 80 °C before extraction. Cell pellets were lysed by the addition with 200 µL Bacterial Protein Extraction Reagent (#78243 Thermo Scientific), 100 µg/mL lysozyme (#L6876 Sigma Aldrich), and 5 µ/mL DNase I (#M0303S New England Biolabs). The total protein abundance of each sample lysate was quantified using a Pierce BCA Protein Assay Kit (#A65453 Thermo Scientific) according to the manufacturer's instructions. Samples were diluted to equal protein concentrations prior to performing the OxiSelect ELISA assay. Absorbance measurements were taken at 450 nm on an Agilent Biotek Synergy H1 microplate reader.

Oxidized deoxyguanosine quantification

Oxidized deoxyguanosine (8-oxo-dG)) was quantified using the OxiSelect Oxidative DNA Damage ELISA kit (#STA-320 Cell Biolabs) according to the manufacturer's instructions, as previously described[135]. Frozen bacterial pellets were obtained as described above for carbonylated protein quantification experiments. Total DNA was extracted using the DNeasy UltraClean Microbial Kit (#10196-4 Qiagen) according to the manufacturer's instructions. DNA concentrations were measured using a NanoDrop One Microvolume UV-Vis Spectrophotometer (Thermo Scientific). Samples were diluted to equal DNA concentrations. Double-strand DNA was converted to single-strand DNA by incubating samples at 95 °C for 5 min and rapidly chilling on ice. Single-strand DNA was digested with 10 units of Nuclease P1 (#M0660S New England Biolabs) before performing 8-oxo-dG measurements using the OxiSelect ELISA kit. Absorbance measurements were taken at 450 nm on an Agilent Biotek Synergy H1 microplate reader.

Mutation rate estimation

Mutation rates were measured using Luria-Delbrück fluctuation tests[68]. Overnight cultures grown in MOPS-rich media were inoculated 1:250,000 into fresh media with or without ciprofloxacin at a final concentration of 8 ng/mL (~ 0.67x MIC). 1 mL of diluted culture (~ 10^3-10^4 CFUs) was dispensed into the wells of a 96-well, v-bottom, square deep well plate. Plates were sealed using Breathe-Easy permeable membranes and incubated for 24 h at 37 °C and 900 rpm shaking. 500 µL stationary phase cultures were plated on LB agar plates ± 100 µg/mL rifampicin. Colonies were enumerated after 24 h of incubation at 37 °C. Rifampicin resistance (Rif^R) CFUs were normalized by total CFUs. Reported values were scaled by 10^8. Fold-induction by ciprofloxacin was calculated by dividing the measured Rif^R/CFU by the median Rif^R/CFU without ciprofloxacin treatment.

(p)ppGpp quantification

Intracellular (p)ppGpp abundance in exponential phase cells was quantified using the S2 RNA-based fluorescent biosensor[76]. Overnight cultures grown in MOPS rich were inoculated 1:500 into fresh media and grown to $OD_{600} \geq 0.1$. Cultures were back-diluted to $OD_{600} = 0.1$, and 1 mM IPTG was added to induce S2 expression. After 1.5 h of induction, 50 µL aliquots were added to 50 µL of MOPS-rich media containing 1 mM IPTG (#I6758 Sigma Aldrich) and 400 µM DFHBI-1T (#SML2697 Sigma Aldrich) in 1.5 mL microcentrifuge tubes such that the final IPTG and DFHBI-1T concentrations were 1 mM and 200 µM, respectively. DFHBI-1T is the cognate dye for the S2 sensor. Tubes were incubated at room temperature in the dark for 1 h before imaging. 1 µL of cells were placed atop a 1.5% agarose pad mounted on a slide and sealed with a coverslip. Cells were imaged on a Nikon Ti2 Eclipse microscope using a 100x oil objective. Fluorescence measurements were taken at 488 nm and 510–531 nm emission. Negative control experiments were conducted by omitting the addition of IPTG or DFHBI-1T. Stationary phase cells ($OD_{600} > 1.5$) were used as positive controls. Background-subtracted single-cell fluorescence intensities were quantified using the MicrobeJ[136] plugin of ImageJ. Reported values are derived from the median fluorescence of $n \geq 100$ cells per replicate.

Stringent response population fraction quantification

The fraction of cells with active stringent response was quantified by flow cytometry using the chromosomally integrated RpoS::mCherry[78] or rmfp::mCherry[17] fluorescent reporters. Overnight cultures grown in MOPS-rich were inoculated 1:500 into fresh media and grown to $OD_{600} \geq 0.2$ for exponential cells or for 24 h (until $OD_{600} \geq 1.5$) for stationary phase cells. Samples were vortexed to remove clumps and analyzed using a FACSymphony A5 flow cytometer (Becton Dickinson), with fluorescence excitation at 561 nm and emission detected through a 602/15 nm bandpass filter. Flow cytometry data were analyzed using FlowJo (Becton Dickinson). mCherry-positive subpopulations were defined as reporter-bearing cells with fluorescence exceeding a threshold gate set so that ≤ 0.5% of negative control pEmpty cells (lacking reporter) exceeded the gate. The percentages of stringent-on cells were calculated as the number of stringent-on cells divided by the total cell count. Data were collected from $n \geq 30{,}000$ per replicate.

Statistical analyses

Statistical significance testing was performed in Prism v10 (GraphPad; San Diego, CA). Normality testing was performed using the Shapiro-Wilk test. Homogeneity of variance testing was performed using the F test or the Bartlett test, where appropriate. All two-sample comparisons were performed using the Mann-Whitney test or the unpaired *t*test. All multiple-sample comparisons were performed by one-way ANOVA with Dunnett's or Šídák's multiple comparison test, Welch's ANOVA with Dunn's multiple comparison tests, or two-way ANOVA with Dunnett's or Šídák's multiple comparison test. The selection of parametric versus non-parametric tests was determined by tests for normality and homogeneity of variance.

Reporting summary

Further information on research design is available in the Nature Portfolio Reporting Summary linked to this article.

Data availability

All data are available in the main text or supplementary materials. RNA sequencing data generated in this study have been deposited in the Sequence Read Archive under BioProject accession code: PRJNA1242271. Source data are provided in this paper.

Code availability

The code used in this study are available at [https://github.com/jasonhyang/Li_2025]

References

1. Murray, C. J. L. et al. Global burden of bacterial antimicrobial resistance in 2019: a systematic analysis. *Lancet* **399**, 629–655 (2022).
2. Darby, E. M. et al. Molecular mechanisms of antibiotic resistance revisited. *Nat. Rev. Microbiol.* https://doi.org/10.1038/s41579-022-00820-y (2022).
3. Almeida Da Silva, P. E. A. & Palomino, J. C. Molecular basis and mechanisms of drug resistance in Mycobacterium tuberculosis: classical and new drugs. *J. Antimicrob. Chemother.* **66**, 1417–1430 (2011).
4. Brauner, A., Fridman, O., Gefen, O. & Balaban, N. Q. Distinguishing between resistance, tolerance and persistence to antibiotic treatment. *Nat. Rev. Microbiol.* **14**, 320–330 (2016).
5. Lewis, K. Persister cells. *Annu. Rev. Microbiol.* **64**, 357–372 (2010).

6. Harms, A., Maisonneuve, E. & Gerdes, K. Mechanisms of bacterial persistence during stress and antibiotic exposure. *Science* **354**, aaf4268 (2016).
7. Balaban, N. Q. et al. Definitions and guidelines for research on antibiotic persistence. *Nat. Rev. Microbiol.* **17**, 441–448 (2019).
8. Bakkeren, E., Diard, M. & Hardt, W.-D. Evolutionary causes and consequences of bacterial antibiotic persistence. *Nat. Rev. Microbiol.* **18**, 479–490 (2020).
9. Levin-Reisman, I. et al. Antibiotic tolerance facilitates the evolution of resistance. *Science* **355**, 826–830 (2017).
10. Pribis, J. P. et al. Gamblers: An Antibiotic-Induced Evolvable Cell Subpopulation Differentiated by Reactive-Oxygen-Induced General Stress Response. *Mol. Cell* **74**, 785–800.e7 (2019).
11. Zhai, Y. et al. ppGpp and RNA-polymerase backtracking guide antibiotic-induced mutable gambler cells. *Mol. Cell* https://doi.org/10.1016/j.molcel.2023.03.003 (2023).
12. Barrett, T. C., Mok, W. W. K., Murawski, A. M. & Brynildsen, M. P. Enhanced antibiotic resistance development from fluoroquinolone persisters after a single exposure to antibiotic. *Nat. Commun.* **10**, 1177 (2019).
13. Baquero, F. & Levin, B. R. Proximate and ultimate causes of the bactericidal action of antibiotics. *Nat. Rev. Microbiol.* **19**, 123–132 (2021).
14. Schrader, S. M., Vaubourgeix, J. & Nathan, C. Biology of antimicrobial resistance and approaches to combat it. *Sci. Transl. Med.* **12**, eaaz6992 (2020).
15. Carvajal-Garcia, J., Samadpour, A. N., Hernandez, Viera, A. J. & Merrikh, H. Oxidative stress drives mutagenesis through transcription-coupled repair in bacteria. *Proc. Natl. Acad. Sci. USA* **120**, e2300761120 (2023).
16. Ragheb, M. N. et al. Inhibiting the Evolution of Antibiotic Resistance. *Mol. Cell* **73**, 157–165 (2019).
17. Zhai, Y. et al. Drugging evolution of antibiotic resistance at a regulatory network hub. *Sci. Adv.* **9**, eadg0188 (2023).
18. Carvajal-Garcia, J. et al. A small molecule that inhibits the evolution of antibiotic resistance. *Nar. Mol. Med.* **1**, ugae001 (2024).
19. Merrikh, H. & Kohli, R. M. Targeting evolution to inhibit antibiotic resistance. *FEBS J.* **287**, 4341–4353 (2020).
20. Pribis, J. P., Zhai, Y., Hastings, P. J. & Rosenberg, S. M. Stress-induced mutagenesis, gambler cells, and stealth targeting antibiotic-induced evolution. *MBio* **13**, e0107422 (2022).
21. Yang, J. H. et al. A white-box machine learning approach for revealing Antibiotic mechanisms of action. *Cell* **177**, 1649–1661 (2019).
22. Cho, H., Uehara, T. & Bernhardt, T. G. Beta-lactam antibiotics induce a lethal malfunctioning of the bacterial cell wall synthesis machinery. *Cell* **159**, 1300–1311 (2014).
23. Lobritz, M. A. et al. Increased energy demand from anabolic-catabolic processes drives β-lactam antibiotic lethality. *Cell Chem. Biol.* **29**, 276–286 (2022).
24. Belenky, P. et al. Bactericidal antibiotics induce toxic metabolic perturbations that lead to cellular damage. *Cell Rep.* **13**, 968–980 (2015).
25. Dwyer, D. J. et al. Antibiotics induce redox-related physiological alterations as part of their lethality. *Proc. Natl. Acad. Sci. USA* **111**, E2100–E2109 (2014).
26. Lobritz, M. A. et al. Antibiotic efficacy is linked to bacterial cellular respiration. *Proc. Natl. Acad. Sci. USA* **112**, 8173–8180 (2015).
27. Kohanski, M. A., Dwyer, D. J., Hayete, B., Lawrence, C. A. & Collins, J. J. A common mechanism of cellular death induced by bactericidal antibiotics. *Cell* **130**, 797–810 (2007).
28. Chapman, A. G., Fall, L. & Atkinson, D. E. Adenylate energy charge in Escherichia coli during growth and starvation. *J. Bacteriol.* **108**, 1072–1086 (1971).
29. Glick, B. R. Metabolic load and heterologous gene expression. *Biotechnol. Adv.* **13**, 247–261 (1995).
30. Hsieh, L. S., Burger, R. M. & Drlica, K. Bacterial DNA supercoiling and [ATP]/[ADP]. Changes associated with a transition to anaerobic growth. *J. Mol. Biol.* **219**, 443–450 (1991).
31. Bonvillain, R. W., Painter, R. G., Ledet, E. M. & Wang, G. Comparisons of resistance of CF and non-CF pathogens to hydrogen peroxide and hypochlorous acid oxidants in vitro. *BMC Microbiol.* **11**, 112 (2011).
32. Sun, Y., Fukamachi, T., Saito, H. & Kobayashi, H. Respiration and the F1Fo-ATPase enhance survival under acidic conditions in Escherichia coli. *PLoS ONE* **7**, e52577 (2012).
33. Snoeck, S., Guidi, C. & De Mey, M. Metabolic burden" explained: stress symptoms and its related responses induced by (over) expression of (heterologous) proteins in Escherichia coli. *Microb. Cell Fact.* **23**, 96 (2024).
34. Chao, Y. P. & Liao, J. C. Metabolic responses to substrate futile cycling in Escherichia coli. *J. Biol. Chem.* **269**, 5122–5126 (1994).
35. Koebmann, B. J., Westerhoff, H. V., Snoep, J. L., Nilsson, D. & Jensen, P. R. The glycolytic flux in Escherichia coli is controlled by the demand for ATP. *J. Bacteriol.* **184**, 3909–3916 (2002).
36. Holm, A. K. et al. Metabolic and transcriptional response to cofactor perturbations in Escherichia coli. *J. Biol. Chem.* **285**, 17498–17506 (2010).
37. Adolfsen, K. J. & Brynildsen, M. P. Futile cycling increases sensitivity toward oxidative stress in Escherichia coli. *Metab. Eng.* **29**, 26–35 (2015).
38. Boecker, S. et al. Deciphering the physiological response of Escherichia coli under high ATP demand. *Mol. Syst. Biol.* **17**, e10504 (2021).
39. Chatterjee, N. & Walker, G. C. Mechanisms of DNA damage, repair, and mutagenesis. *Environ. Mol. Mutagen.* **58**, 235–263 (2017).
40. Rittershaus, E. S. C., Baek, S.-H. & Sassetti, C. M. The normalcy of dormancy: common themes in microbial quiescence. *Cell Host Microbe* **13**, 643–651 (2013).
41. Conlon, B. P. et al. Persister formation in Staphylococcus aureus is associated with ATP depletion. *Nat. Microbiol.* **1**, 16051 (2016).
42. Shan, Y. et al. ATP-Dependent persister formation in Escherichia coli. *MBio* **8**, e02267–16 (2017).
43. Manuse, S. et al. Bacterial persisters are a stochastically formed subpopulation of low-energy cells. *PLoS Biol.* **19**, e3001194 (2021).
44. Amato, S. et al. The role of metabolism in bacterial persistence. *Front. Microbiol.* **5**, 70 (2014).
45. Li, B., Chen, X., Yang, J.-Y., Gao, S. & Bai, F. Intracellular ATP concentration is a key regulator of bacterial cell fate. *J. Bacteriol.* **206**, e0020824 (2024).
46. Stokes, J. M., Lopatkin, A. J., Lobritz, M. A. & Collins, J. J. Bacterial metabolism and antibiotic efficacy. *Cell Metab.* **30**, 251–259 (2019).
47. Ahmad, M., Aduru, S. V., Smith, R. P., Zhao, Z. & Lopatkin, A. J. The role of bacterial metabolism in antimicrobial resistance. *Nat. Rev. Microbiol.* https://doi.org/10.1038/s41579-025-01155-0 (2025).
48. McCloskey, D., Xu, J., Schrübbers, L., Christensen, H. B. & Herrgård, M. J. RapidRIP quantifies the intracellular metabolome of 7 industrial strains of E. coli. *Metab. Eng.* **47**, 383–392 (2018).
49. McCloskey, D. et al. A model-driven quantitative metabolomics analysis of aerobic and anaerobic metabolism in E. coli K-12 MG1655 that is biochemically and thermodynamically consistent. *Biotechnol. Bioeng.* **111**, 803–815 (2014).
50. Atkinson, D. E. The energy charge of the adenylate pool as a regulatory parameter. Interaction with feedback modifiers. *Biochemistry* **7**, 4030–4034 (1968).
51. Williamson, D. H., Lund, P. & Krebs, H. A. The redox state of free nicotinamide-adenine dinucleotide in the cytoplasm and mitochondria of rat liver. *Biochem. J.* **103**, 514–527 (1967).

52. Atkinson, D. E. *Cellular Energy Metabolism and Its Regulation*. (Academic Press, San Diego, CA, 1977).
53. Nelson, D. L. & Cox, M. M. *Lehninger Principles of Biochemistry*. (W. H. Freeman, 2021).
54. Walsh, C. T., Tu, B. P. & Tang, Y. Eight kinetically stable but thermodynamically activated molecules that power cell metabolism. *Chem. Rev.* **118**, 1460–1494 (2018).
55. Clinical and Laboratory Standards Institute. *Performance Standards for Antimicrobial Susceptibility Testing, 35th Ed. CLSI Guideline M100* (2025).
56. Shatalin, K., Shatalina, E., Mironov, A. & Nudler, E. H2S: a universal defense against antibiotics in bacteria. *Science* **334**, 986–990 (2011).
57. Shatalin, K. et al. Inhibitors of bacterial H2S biogenesis targeting antibiotic resistance and tolerance. *Science* **372**, 1169–1175 (2021).
58. Wadhams, G. & Armitage, J. Making sense of it all: bacterial chemotaxis. *Nat. Rev. Mol. Cell Biol.* **5**, 1024–1037 (2004).
59. Sowa, Y. & Berry, R. M. Bacterial flagellar motor. *Q. Rev. Biophys* (2008).
60. O'Brien, E. J., Monk, J. M. & Palsson, B. O. Using genome-scale models to predict biological capabilities. *Cell* **161**, 971–987 (2015).
61. Shlomi, T., Cabili, M. N., Herrgård, M. J., Palsson, B. Ø & Ruppin, E. Network-based prediction of human tissue-specific metabolism. *Nat. Biotechnol.* **26**, 1003–1010 (2008).
62. Zur, H., Ruppin, E. & Shlomi, T. iMAT: an integrative metabolic analysis tool. *Bioinformatics* **26**, 3140–3142 (2010).
63. Monk, J. M. et al. iML1515, a knowledgebase that computes Escherichia coli traits. *Nat. Biotechnol.* **35**, 904–908 (2017).
64. Seaver, L. C. & Imlay, J. A. Alkyl hydroperoxide reductase is the primary scavenger of endogenous hydrogen peroxide in Escherichia coli. *J. Bacteriol.* **183**, 7173–7181 (2001).
65. Tanaka, K., Handel, K., Loewen, P. C. & Takahashi, H. Identification and analysis of the rpoS-dependent promoter of katE, encoding catalase HPII in Escherichia coli. *Biochim. Biophys. Acta* **1352**, 161–166 (1997).
66. Takahashi, N. et al. Lethality of MalE-LacZ hybrid protein shares mechanistic attributes with oxidative component of antibiotic lethality. *Proc. Natl. Acad. Sci. USA* **114**, 9164–9169 (2017).
67. Sakai, A., Nakanishi, M., Yoshiyama, K. & Maki, H. Impact of reactive oxygen species on spontaneous mutagenesis in Escherichia coli. *Genes Cells* **11**, 767–778 (2006).
68. Luria, S. E. & Delbrück, M. Mutations of bacteria from virus sensitivity to virus resistance. *Genetics* **28**, 491–511 (1943).
69. Jones, M. E., Thomas, S. M. & Rogers, A. Luria-Delbrück fluctuation experiments: design and analysis. *Genetics* **136**, 1209–1216 (1994).
70. Jensen, P. R. & Michelsen, O. Carbon and energy metabolism of atp mutants of Escherichia coli. *J. Bacteriol.* **174**, 7635–7641 (1992).
71. Portnoy, V. A., Herrgård, M. J. & Palsson, B. Ø Aerobic fermentation of d -glucose by an evolved cytochrome oxidase-deficient Escherichia coli strain. *Appl. Environ. Microbiol.* **74**, 7561–7569 (2008).
72. Perlin, D. S., Latchney, L. R. & Senior, A. E. Inhibition of Escherichia coli H+-ATPase by venturicidin, oligomycin and ossamycin. *Biochim. Biophys. Acta* **807**, 238–244 (1985).
73. Sekiya, M., Nakamoto, R. K., Nakanishi-Matsui, M. & Futai, M. Binding of phytopolyphenol piceatannol disrupts β/γ subunit interactions and rate-limiting step of steady-state rotational catalysis in Escherichia coli F1-ATPase. *J. Biol. Chem.* **287**, 22771–22780 (2012).
74. Irving, S. E., Choudhury, N. R. & Corrigan, R. M. The stringent response and physiological roles of (pp)pGpp in bacteria. *Nat. Rev. Microbiol.* **19**, 256–271 (2021).
75. Balaban, N. Q., Merrin, J., Chait, R., Kowalik, L. & Leibler, S. Bacterial persistence as a phenotypic switch. *Science* **305**, 1622–1625 (2004).
76. Sun, Z. et al. Live-cell imaging of guanosine tetra- and penta-phosphate (p)ppGpp with RNA-based fluorescent sensors*. *Angew. Chem. Int. Ed. Engl.* **60**, 24070–24074 (2021).
77. Filonov, G. S., Moon, J. D., Svensen, N. & Jaffrey, S. R. Broccoli: rapid selection of an RNA mimic of green fluorescent protein by fluorescence-based selection and directed evolution. *J. Am. Chem. Soc.* **136**, 16299–16308 (2014).
78. Svenningsen, M. S., Veress, A., Harms, A., Mitarai, N. & Semsey, S. Birth and resuscitation of (p)ppGpp induced antibiotic tolerant persister cells. *Sci. Rep.* **9**, 6056 (2019).
79. Hara, K. Y. & Kondo, A. ATP regulation in bioproduction. *Microb. Cell Fact.* **14**, 198 (2015).
80. Mori, M., Cheng, C., Taylor, B. R., Okano, H. & Hwa, T. Functional decomposition of metabolism allows a system-level quantification of fluxes and protein allocation towards specific metabolic functions. *Nat. Commun.* **14**, 4161 (2023).
81. Russell, J. B. & Cook, G. M. Energetics of bacterial growth: balance of anabolic and catabolic reactions. *Microbiol. Rev.* **59**, 48–62 (1995).
82. Monod, J. *Recherches sur la Croissance des Cultures Bactériennes*. (University of Paris, Paris, France, 1942).
83. Foti, J. J., Devadoss, B., Winkler, J. A., Collins, J. J. & Walker, G. C. Oxidation of the guanine nucleotide pool underlies cell death by bactericidal antibiotics. *Science* **336**, 315–319 (2012).
84. Ponder, R. G., Fonville, N. C. & Rosenberg, S. M. A switch from high-fidelity to error-prone DNA double-strand break repair underlies stress-induced mutation. *Mol. Cell* **19**, 791–804 (2005).
85. Hasegawa, K., Yoshiyama, K. & Maki, H. Spontaneous mutagenesis associated with nucleotide excision repair in Escherichia coli. *Genes Cells* **13**, 459–469 (2008).
86. Lopatkin, A. J. et al. Bacterial metabolic state more accurately predicts antibiotic lethality than growth rate. *Nat. Microbiol.* **4**, 2109–2117 (2019).
87. Gutierrez, A. et al. Understanding and sensitizing density-dependent persistence to quinolone antibiotics. *Mol. Cell* **68**, 1147–1154.e3 (2017).
88. Pontes, M. H. & Groisman, E. A. Slow growth determines nonheritable antibiotic resistance in Salmonella enterica. *Sci. Signal.* **12**, eaax3938 (2019).
89. Pontes, M. H. & Groisman, E. A. A physiological basis for nonheritable antibiotic resistance. *MBio* **11**, e00817–e00820 (2020).
90. Chen, C. R., Malik, M., Snyder, M. & Drlica, K. DNA gyrase and topoisomerase IV on the bacterial chromosome: quinolone-induced DNA cleavage. *J. Mol. Biol.* **258**, 627–637 (1996).
91. Amato, S. M., Orman, M. A. & Brynildsen, M. P. Metabolic control of persister formation in Escherichia coli. *Mol. Cell* **50**, 475–487 (2013).
92. Ocampo, P. S. et al. Antagonism between bacteriostatic and bactericidal antibiotics is prevalent. *Antimicrob. Agents Chemother.* **58**, 4573–4582 (2014).
93. Prasetyoputri, A., Jarrad, A. M., Cooper, M. A. & Blaskovich, M. A. T. The Eagle effect and antibiotic-induced persistence: Two sides of the same coin?. *Trends Microbiol.* **27**, 339–354 (2019).
94. Eagle, H. & Musselman, A. The rate of bactericidal action of penicillin in vitro as a function of its concentration, and its paradoxically reduced activity at high concentrations against certain organisms. *J. Exp. Med.* **88**, 99–131 (1948).
95. Piddock, L. J., Walters, R. N. & Diver, J. M. Correlation of quinolone MIC and inhibition of DNA, RNA, and protein synthesis and induction of the SOS response in Escherichia coli. *Antimicrob. Agents Chemother.* **34**, 2331–2336 (1990).
96. El Khoury, J. Y., Zamarreño Beas, J., Huguenot, A., Py, B. & Barras, F. Bioenergetic state of Escherichia coli controls aminoglycoside susceptibility. *MBio* **14**, e0330222 (2023).

97. García-Villada, L., Degtyareva, N. P., Brooks, A. M., Goldberg, J. B. & Doetsch, P. W. A role for the stringent response in ciprofloxacin resistance in Pseudomonas aeruginosa. *Sci. Rep.* **14**, 8598 (2024).
98. Qi, W., Jonker, M. J., de Leeuw, W., Brul, S. & Ter Kuile, B. H. Role of RelA-synthesized (p)ppGpp and ROS-induced mutagenesis in de novo acquisition of antibiotic resistance in E. coli. *iScience* **27**, 109579 (2024).
99. Wright, B. E. The effect of the stringent response on mutation rates in Escherichia coli K-12. *Mol. Microbiol.* **19**, 213–219 (1996).
100. Windels, E. M. et al. Bacterial persistence promotes the evolution of antibiotic resistance by increasing survival and mutation rates. *ISME J.* **13**, 1239–1251 (2019).
101. Mathieu, A. et al. Discovery and function of a general core hormetic stress response in E. coli induced by sublethal concentrations of antibiotics. *Cell Rep.* **17**, 46–57 (2016).
102. M. Fruci & K. in *Stress and Environmental Regulation of Gene Expression and Adaptation in Bacteria* 115–136 (John Wiley & Sons, Inc., Hoboken, NJ, USA, 2016).
103. Gruber, C. C. & Walker, G. C. Incomplete base excision repair contributes to cell death from antibiotics and other stresses. *DNA Repair* **71**, 108–117 (2018).
104. Wyrzykowski, J. & Volkert, M. R. The Escherichia coli methyl-directed mismatch repair system repairs base pairs containing oxidative lesions. *J. Bacteriol.* **185**, 1701–1704 (2003).
105. Bradbury, J. D. et al. Development of an inhibitor of the mutagenic SOS response that suppresses the evolution of quinolone antibiotic resistance. *Chem. Sci.* **15**, 9620–9629 (2024).
106. Bollenbach, T., Quan, S., Chait, R. & Kishony, R. Nonoptimal microbial response to antibiotics underlies suppressive drug interactions. *Cell* **139**, 707–718 (2009).
107. Cokol, M. et al. Systematic exploration of synergistic drug pairs. *Mol. Syst. Biol.* **7**, 544 (2011).
108. Sakenova, N. et al. Systematic mapping of antibiotic cross-resistance and collateral sensitivity with chemical genetics. *Nat. Microbiol.* https://doi.org/10.1038/s41564-024-01857-w (2024).
109. Zeng, J. et al. A broadly applicable, stress-mediated bacterial death pathway regulated by the phosphotransferase system (PTS) and the cAMP-Crp cascade. *Proc. Natl. Acad. Sci. USA* **119**, e2118566119 (2022).
110. Li, L. et al. Systematic analyses identify modes of action of ten clinically relevant biocides and antibiotic antagonism in Acinetobacter baumannii. *Nat. Microbiol.* **8**, 1995–2005 (2023).
111. Yang, J. H. et al. Antibiotic-induced changes to the host metabolic environment inhibit drug efficacy and alter immune function. *Cell Host Microbe* **22**, 757–765.e3 (2017).
112. Hernandez-Morfa, M. et al. Host cell oxidative stress promotes intracellular fluoroquinolone persisters of Streptococcus pneumoniae. *Microbiol. Spectr.* **10**, e0436422 (2022).
113. Helaine, S., Conlon, B. P., Davis, K. M. & Russell, D. G. Host stress drives tolerance and persistence: The bane of anti-microbial therapeutics. *Cell Host Microbe* **32**, 852–862 (2024).
114. Russell, D. G. Who puts the tubercle in tuberculosis?. *Nat. Rev. Microbiol.* **5**, 39–47 (2007).
115. Wu, G. et al. Metabolic burden: Cornerstones in synthetic biology and metabolic engineering applications. *Trends Biotechnol.* **34**, 652–664 (2016).
116. Cardinale, S. & Arkin, A. P. Contextualizing context for synthetic biology-identifying causes of failure of synthetic biological systems. *Biotechnol. J.* **7**, 856–866 (2012).
117. Johnson, E. T. & Schmidt-Dannert, C. Light-energy conversion in engineered microorganisms. *Trends Biotechnol.* **26**, 682–689 (2008).
118. Ceroni, F., Algar, R., Stan, G.-B. & Ellis, T. Quantifying cellular capacity identifies gene expression designs with reduced burden. *Nat. Methods* **12**, 415–418 (2015).
119. Baba, T. et al. Construction of Escherichia coli K-12 in-frame, single-gene knockout mutants: the Keio collection. *Mol. Syst. Biol.* **2**, 2006.0008 (2006).
120. Cherepanov, P. P. & Wackernagel, W. Gene disruption in Escherichia coli: TcR and KmR cassettes with the option of Flp-catalyzed excision of the antibiotic-resistance determinant. *Gene* **158**, 9–14 (1995).
121. Lopatkin, A. J. et al. Clinically relevant mutations in core metabolic genes confer antibiotic resistance. *Science* **371**, eaba0862 (2021).
122. McCloskey, D., Gangoiti, J. A., Palsson, B. O. & Feist, A. M. A pH and solvent optimized reverse-phase ion-paring-LC–MS/MS method that leverages multiple scan-types for targeted absolute quantification of intracellular metabolites. *Metabolomics* **11**, 1338–1350 (2015).
123. Su, X. et al. In-source CID ramping and covariant ion analysis of hydrophilic interaction chromatography metabolomics. *Anal. Chem.* **92**, 4829–4837 (2020).
124. McCloskey, D., Utrilla, J., Naviaux, R. K., Palsson, B. O. & Feist, A. M. Fast Swinnex filtration (FSF): a fast and robust sampling and extraction method suitable for metabolomics analysis of cultures grown in complex media. *Metabolomics* **11**, 198–209 (2015).
125. Melamud, E., Vastag, L. & Rabinowitz, J. D. Metabolomic analysis and visualization engine for LC-MS data. *Anal. Chem.* **82**, 9818–9826 (2010).
126. Langmead, B. & Salzberg, S. L. Fast gapped-read alignment with Bowtie 2. *Nat. Methods* **9**, 357–359 (2012).
127. Liao, Y., Smyth, G. K. & Shi, W. FeatureCounts: An efficient general purpose program for assigning sequence reads to genomic features. *Bioinformatics* **30**, 923–930 (2014).
128. Hicks, S. C. et al. Smooth quantile normalization. *Biostatistics* **19**, 185–198 (2018).
129. Ewels, P., Magnusson, M., Lundin, S. & Käller, M. MultiQC: summarize analysis results for multiple tools and samples in a single report. *Bioinformatics* **32**, 3047–3048 (2016).
130. Love, M. I., Huber, W. & Anders, S. Moderated estimation of fold change and dispersion for RNA-seq data with DESeq2. *Genome Biol.* **15**, 550 (2014).
131. Thomas, P. D. et al. PANTHER: Making genome-scale phylogenetics accessible to all. *Protein Sci.* **31**, 8–22 (2022).
132. Benjamini, Y. & Hochberg, Y. Controlling the false discovery rate: A practical and powerful approach to multiple testing. *J. R. Stat. Soc. Ser. B: Stat. Methodol.* **57**, 289–300 (1995).
133. Ebrahim, A., Lerman, J. A., Palsson, B. O. & Hyduke, D. R. COBRApy: COnstraints-based reconstruction and analysis for Python. *BMC Syst. Biol.* **7**, 74 (2013).
134. Megchelenbrink, W., Huynen, M. & Marchiori, E. OptGpSampler: An improved tool for uniformly sampling the solution-space of genome-scale metabolic networks. *PLoS ONE* **9**, e86587 (2014).
135. Ofori-Anyinam, B. et al. Catalase activity deficiency sensitizes multidrug-resistant Mycobacterium tuberculosis to the ATP synthase inhibitor bedaquiline. *Nat. Commun.* **15**, 1–13 (2024).
136. Ducret, A., Quardokus, E. & Brun, Y. MicrobeJ, a tool for high throughput bacterial cell detection and quantitative analysis. *Nat. Microbiol.* **1**, 16077–16077 (2016).

Acknowledgements

We thank the Rutgers Genomics Center for support in sequencing RNA. We thank Alexander Harms (ETH Zurich) for sharing RpoS::mCherry. We thank Susan Rosenberg (Baylor College of Medicine) for sharing rmfp::mCherry. We thank Matthew Neiditch for sharing *E. coli* BL21(DE3). We thank James Imlay (University of Illinois, Urbana-Champaign), Allison Lopatkin (University of Rochester), Susan Rosenberg (Baylor College of Medicine), and Houra Merrikh (Vanderbilt University) for helpful discussions. This work was supported by National Institutes of Health grants R00-GM118907, U19-AI162598, and R01-AI146194, Rutgers University Busch Biomedical Grant, and the Agilent Early Career Professor

Award to J.H.Y., P30-CA072720 to the Rutgers Cancer Institute Metabolomics Shared Resource (X.S.), and Novo Nordisk Foundation Grant NNF10CC1016517 to D.M.

Author contributions

B.L. and J.H.Y. conceptualized the study. B.L., S.S., M.S., G.M., M.R.G., A.S., E.N.C., B.O., T.C., N.J.C., D.M., and J.H.Y. executed experiments. B.L. and J.H.Y. analyzed and visualized the data and wrote the manuscript. X.S. and J.H.Y. supervised the study.

Competing interests

The authors declare no competing interests.

Additional information

Supplementary information The online version contains supplementary material available at https://doi.org/10.1038/s41467-025-60302-6.

Correspondence and requests for materials should be addressed to Jason H. Yang.

Peer review information *Nature Communications* thanks Niclas Nordholt and the other anonymous reviewers for their contribution to the peer review of this work. A peer review file is available.